Supplemental Information

# Radium Accumulation in Carbonate River Sediments at Oil and Gas Produced Water Discharges: Implications for Beneficial Use as Disposal Management

Bonnie McDevitt[a], Molly McLaughlin[b], Charles A. Cravotta III[c], Moses A. Ajemigbitse[a], Katherine J. Van Sice[a], Jens Blotevogel[b], Thomas Borch[bde], Nathaniel R. Warner[a1]

[a] Civil and Environmental Engineering Department, The Pennsylvania State University, University Park, PA 16802

[b]Department of Civil and Environmental Engineering, Colorado State University, 1320 Campus Delivery, Fort Collins, Colorado 80523, United States

[c] U.S. Geological Survey, Pennsylvania Water Science Center, 215 Limekiln Road, New Cumberland, PA 17070

[d]Department of Soil and Crop Sciences, Department of Soil and Crop Sciences, Colorado State University, 1170 Campus Delivery, Fort Collins, Colorado 80523, United States

[e]Department of Chemistry, Colorado State University, 1872 Campus Delivery, Fort Collins, Colorado 80523, United States

[1] Corresponding author: nrw6@spu.edu

## Supplemental Materials and Methods

*Wyoming, USA Study Site Description*

This investigation focused on a large river basin in Wyoming that contains two major perennial rivers (B and C) and a naturally ephemeral tributary (A) (Figure 1 of paper). The precise locations are not disclosed in accordance with access agreements with private land owners. All four streams flow into a reservoir that ultimately stores water used for irrigation and drinking water by the local municipality. Increasing TDS downstream of produced water stream confluence points in rivers B and C caused concern for high TDS loads from NPDES-permitted discharges and provided motivation to start frequent water sampling in 2013.

The study area is located within the Wyoming Basin ecoregion and is mainly comprised of rolling plains of sagebrush and mixed grass prairie surrounded by low mountains of elevation ranging from 1500-2000 meters. Oil, gas, coal, uranium and bentonite deposits are common throughout the region as are gypsum-dominated soils. Much of the plains are utilized for livestock grazing and wildlife habitat such as for wild horses. Areas located close to the perennial rivers sustain irrigated grass hay fields due to various dams and diversions that channel water, especially prevalent along River B.

The study area climate ranges from arid to semi-arid with total precipitation from 2013-2016 ranging from 181 mm of rain per year in the plains to 545 mm closer to the alpine foothills. Precipitation data for the study period were collected from three regional stations property of the National Oceanic and Atmospheric Administration National Weather Service for Wyoming (http://www.weather.gov/). Stream gauge discharge data for all three river systems for the water years 2013 to 2016 were accessed through the publicly available USGS National Water Information System (https://waterdata.usgs.gov/nwis/rt). Hydrographs showing sampling conditions are shown in Figure S2.

Tributary A represents an ephemeral tributary to the larger River B. The tributary drains an area of 1083 $km^2$ and channels both NPDES produced water discharges in its headwaters and irrigation return flows. Four NPDES discharge facilities dispose wastewater in Tributary A headwaters. Four sample sites were located along the produced water stream formed from the discharges and four were located on the larger Tributary A, spanning a total distance of approximately 68 km from furthest upstream NPDES discharge, DA-1, to most downstream Tributary site, A4. Sites DA-1, DA-2, and DA-3 were located just below discharges. Annual mean stream flows ranged very little from 4.19-4.98 cubic meter per second ($m^3/s$) from 2013-2016.

River B was the largest of the streams sampled flowing 298 km and draining 5980 $km^2$. Four NPDES-permitted facilities were sampled on a major O&G field on an ephemeral tributary to River B north of sample site B-3. Two of the facilities, owned by the same operator, were sampled directly at the point of discharge while the other two were not consistently discharging produced water over the study period and one became repurposed as a reinjection facility. Facility DB-2.0 was only sampled once immediately downstream of the discharge outfall in October 2016 for both water quality analysis and grab sediment. Sample distance spanned 64 km between facility DB-1.0 and the confluence with River B. Annual mean stream flows ranged from 7.62-42.14 $m^3/s$ from 2013-2016.

River C was a smaller perennial river, eventually flowing into River B, which drained an area of 4931 $km^2$. One NPDES-permitted facility, DC-1, was sampled directly at point of discharge on an ephemeral tributary to the river along with three sample sites located along the produced water stream to the confluence with River C. Often, the produced water stream dried completely before reaching the River C confluence. Three river sites were sampled above and below the confluence, C1, C2 and C3. The distance spanned from DC-1 to River C was approximately 32 km. Annual mean stream flow values increased steadily from 6.48-20 $m^3/s$ over the period 2013-2016.

*Geochemical Modeling*

To evaluate potential chemical changes resulting from the progressive evaporation of the NPDES - permitted discharges along downstream flow paths, four different forward-reaction scenarios were simulated for samples collected in October 2016 at DB-2.0 and at DC-1: (1) evaporation without reactions; (2) evaporation plus precipitation of pure mineral phases; (3) evaporation plus precipitation of pure mineral and binary solid-solution phases; and (4) evaporation, solid-phase precipitation, plus adsorption of radium, barium, strontium, and other ions by hydrous ferric oxide (HFO) and hydrous manganese oxide (HMO). All four scenarios were modeled using the "phreeqc.dat" data base augmented with thermodynamic data for radium species and phases from "sit.dat". For scenarios 3 and 4, binary solid solutions consisting of barite and $RaSO_4$ ($(Ba, Ra)SO_4$) or aragonite and $RaCO_3$ ($(Ca, Ra)CO_3$), were evaluated. For the current evaluation, model versions considered ideal (default) and non-ideal mixing for the binary solid solutions. Dimensionless Guggenheim mixing parameters for non-ideal binary solid solutions of strontium in barite or aragonite were adopted from Glynn (2000); for the radium solid-solutions radium was substituted for strontium in the formulas.[1] The first three scenarios were also modeled using the "pitzer.dat" data base provided with PHREEQC 3.4.0 augmented with Pitzer parameters for radium species from Rosenburg et al. (2011); however, when using the Pitzer data base, adsorption by HFO and HMO considered in scenario 4 could not be evaluated.[2,3] Note that the ionic strength of the simulated evaporated solutions retained greater than 50 percent of the initial water and the maximum value of ionic strength of all collected water samples (0.18 mol/L) were well below that of seawater, 0.7 mol/L.[4] Thus, aqueous speciation computations using the default activity correction methods with the phreeqc.dat or wateq4f.dat data base in PHREEQC would be appropriate for evaluation of observed sample characteristics.

Adsorption simulations employed the monoprotic, diffuse double layer (MDDL) model of Dzombak and Morel (1990) with surface binding coefficients for radium and barium on HFO reported by Sajih et al (2014).[5,6] The binding coefficients for barium and strontium on HMO were adopted from Tonkin et al. (2004), and that for radium on HMO was estimated using its first hydrolysis constant and linear free energy relation (LFER) reported by Pourret and Davranche (2013) based on the data of Tonkin et al. (2004).[7,8]

Simulation results for pH, solute concentrations, and mass removed by precipitation and, if considered, adsorption for each scenario were displayed as a function of the fraction of water remaining, which is the inverse of the concentration factor (Table S6), and compared with measured aqueous

concentration data for $SO_4$, Cl, Ca, Ba, Sr, and Ra in the initial discharge and downstream waters. The fraction of water remaining in the downstream water samples was estimated as the ratio of the starting Cl concentration divided by the respective downstream concentration. Example PHREEQC codes used for the above simulations and selected graphical results are appended to this Supplemental Information.

*Statistical Analysis*

Regression analysis, ANOVA, Pairwise Wilcoxon rank sum, and Kruskal-Wallis rank sum statistical tests for significance were determined using R statistical software (Version 0.99.486).

**Supplemental Results**

Our evaluations of the progressive evaporation downstream of discharges indicates that the removal of water and precipitation of solids as they reach saturation generally can explain the observed downstream trends.

*Geochemical Modeling*

The PHREEQC saturation index results indicate consistent saturation or supersaturation of the discharges and downstream waters with respect to calcite, aragonite, and dolomite ($CaMg(CO_3)_2$), plus barite (Figure S6). Saturation indices for the ideal solid-solutions $(Ca,Ra)CO_3$ and $(Ba,Ra)SO_4$, plus $(Ba,Sr,Ra)SO_4$, exhibited the same magnitude and trends as those for the major end-member solids (Figures S6 G-I). In River B, strontianite ($SrCO_3$) and celestite were supersaturated at discharges (DB-2.0 and DB-4.0) as compared to the larger river and the other stream systems. River C discharges from facility DC-1 also had strontianite saturation indices above equilibrium with decreasing values downstream, possibly resulting from the removal of carbonate ion by precipitation of aragonite, calcite, and dolomite. Tributary A maintained saturation indices relatively constant from discharges to downstream though gypsum ($CaSO_4{:}2H_2O$) and celestite changed from being more undersaturated upstream to almost equilibrium further downstream at tributary sites, consistent with evaporation progressively increasing TDS, SC, and osmotic pressure along the flow path. Downstream river waters generally were undersaturated with respect to gypsum, celestite, and strontianite.

Figures S7 and S8 show the results for the same evaporation models, but for different two starting solutions, DB-2.0 and DC-1 discharges. The conservative evaporation model for discharge DB-2.0 to a tributary on River B adequately explains the observed increases in SC and concentrations of TDS, Cl, and, to a lesser extent, $SO_4$ and Sr downstream of the discharge, but fails to explain the observed changes in pH and corresponding concentrations of Ca, Ba, and Ra (Figure S7 A,C,E), whose concentrations are less than

predicted by simple evaporation. The model that combines evaporation with geochemical reactions, including equilibration with the atmosphere and precipitation of ideal $(CaRa)CO_3$ and $(BaRa)SO_4$ solid-solutions, effectively simulates the observed changes in pH, Ca, and Ra, including the general trends for Ba, but overpredicts the removal of Sr and, especially, Ba (Fig. S7 B,D,F). Additional simulations, which are not illustrated, indicated that (1) increasing barite solubility by 0.5 log units or (2) adsorption of Ba and Sr by 100 mg/L each of HFO and HMO had a negligible effect on the potential for Ra attenuation or associated mineral precipitation. Although large additions of HMO sorbent could effectively bind $Ba^{2+}$ and $Sr^{2+}$, decreasing the corresponding saturation states for minerals such as barite and celestite (e.g. Van Sice et al, in press), available data on the stream sediments indicate very low concentrations of Fe and Mn and, thus, do not support further modifications for consideration of adsorption.

Using the starting solution composition for DC-1 with the initial model for DB-2.0 that combined evaporation with equilibrium reactions, including precipitation of ideal $(Ca,Ra)CO_3$ and $(Ba,Ra)SO_4$ solid-solutions, provided reasonable prediction of the observed trends for SC and concentrations of TDS, Cl, and $SO_4$, downstream of the discharge. Results for pH, Ca, and Sr were improved by expanding the model to use the REACTION_TEMPERATURE block to simulate changes in water temperature from 38˚C at the discharge to 25˚C and then 8˚C at the downstream sites. Additional adjustment of the Guggenheim parameter value from 1.0 to 3.5 for $(Ba,Ra)SO_4$, which decreased the mole fraction of $RaSO_4$ co-precipitated with barite, resulted in reasonable simulation of the observed changes in Ra (Figure S8 B,D,F). Although the model results overpredicted removal of Ba by an order of magnitude, further adjustments to equilibrium constants or adsorbent quantities were not justifiable to simulate observed disequilibrium for barium (Figures S8, E,F,H,I).

For both the evaporation models of DB-2.0 (Figure S7) and DC-1 (Figure S8), radium attenuation resulted from its co-precipitation with aragonite and barite, as $(Ca,Ra)CO_3$ and $(Ba,Ra)SO_4$ solid solutions, respectively. In both cases, the estimated mole fraction of $RaCO_3$ in $(Ca,Ra)CO_3$ was 4 to 6 orders of magnitude less than the corresponding mole fraction of $RaSO_4$ in $(Ba,Ra)SO_4$ (Figure S9 C,D). Nevertheless, for conditions where at least 10 percent of the water remained during evaporation, the estimated mass of $(Ca,Ra)CO_3$ precipitated was approximately 3 orders of magnitude greater than that of $(Ba,Ra)SO_4$ (Figure S9 A,B). For extreme evaporation conditions, where less than 10 percent of the initial water remained, gypsum precipitation resulted in undersaturation with respect to calcium carbonate phases. Thus, the indicated removal of radium with aragonite and the relative abundance of the carbonate phase among the precipitated solids at more upstream locations would be substantial, as indicated by XRD of sediments (Fig. 6). Considering that the evaporation models overpredict the removal of barium by nearly an order of

magnitude compared to measured concentrations at the downstream sample locations, the computed mass of (Ba,Ra)$SO_4$ precipitated and the corresponding fraction of radium removed with the sulfate solid-solution phase will be overpredicted. Consequently, removal of radium with the carbonate phase may be underpredicted, as the radium in solution would be available to precipitate as (Ca,Ra)$CO_3$.

The computed ionic contributions to SC indicate downstream trends that are consistent with the evaporation and geochemical reaction models. Specifically, as shown in Figure S10, relative contributions of calcium, bicarbonate, and carbonate to SC decrease downstream of the NPDES-permitted discharge samples, consistent with removal of these ions along the flow path by carbonate mineral precipitation. In contrast, the relative contributions of sodium and chloride to SC increase downstream, owing to evaporation, while those of sulfate may increase or decrease. Downstream of DC-1 sulfate and sodium sulfate contributions increased, whereas they remained relatively constant downstream of DB-2.0, consistent with extensive evaporation (50% of water remaining) combined with precipitation of sulfate mineral phases for the latter.

*Grain Size*

Percentages of each grain-size did not correlate with the total radium activities in sediments (Figure S13) as has been reported in studies on radium associations with barite in the ultra-fine grained silt-clay fraction of sediments.[9,10] As there are few barite or clay minerals present near high activity discharge sediments this could be expected. Except for DC-1, all grain-sized samples did have increasing $^{226}$Ra activities from the coarse sand to silt-clay fractions. DC-1 grain-sized sediments had an even distribution of $^{226}$Ra activity throughout the sizes with coarse sand containing 0.53 Bq compared to 0.46 Bq in the fine sand and 0.49 Bq in the silt-clay.

**Disclaimer**

Any use of trade, firm, or product names is for descriptive purposes only and does not imply endorsement by the U.S. Government.

**Supplemental References**


1 P. Glynn, Solid-solution solubilities and thermodynamics: Sulfates, carbonates and halides, *Rev. Mineral. Geochemistry*, 2000, **40**, 481–511.

2 D. L. Parkhurst and C. A. J. Appelo, Description of Input and Examples for PHREEQC Version 3 — A Computer Program for Speciation, Batch-Reaction, One-Dimensional Transport, and Inverse Geochemical Calculations. *U.S. Geol. Surv. Tech. Methods, B. 6, chapter A43*, 2013.

3 Y. O. Rosenberg, V. Metz and J. Ganor, Co-precipitation of radium in high ionic strength systems: Thermodynamic properties of the Na-Ra-Cl-$SO_4$-$H_2O$ system - Estimating Pitzer parameters for $RaCl_2$, *Geochim. Cosmochim. Acta*, 2011, **75**, 5389–5402.

4 D. K. Nordstrom, L. N. Plummer, T. M. L. Wigley, T. J. Wolery, J. W. Ball, E. A. Jenne, R. L. Bassett, D. A. Crerar, T. M. Florence, B. Fritz, M. Hoffman, G. R. Holdren, G. M. Lafon, S. V. Mattigod, R. E. McDuff, F. Morel, M. M. Reddy, G. Sposito and J. Thrailkill, A comparison of computerized chemical models for equilibrium calculations in aqueous systems, In E. A. Jenne, ed., *Chemical modeling in aqueous systems--Speciation, sorption, solubility, and kinetics*. American Chemical Society Symposium Series 93, p. 857-892, 1979.

5 D. A. Dzombak and M. M. Morel, *Surface Complexation Modeling: Hydrous ferric oxide*, Wiley-Interscience, 1990.

6 M. Sajih, N. D. Bryan, F. R. Livens, D. J. Vaughan, M. Descostes, V. Phrommavanh, J. Nos and K. Morris, Adsorption of radium and barium on goethite and ferrihydrite: A kinetic and surface complexation modelling study, *Geochim. Cosmochim. Acta*, 2014, **146**, 150–163.

7 J. W. Tonkin, L. S. Balistrieri and J. W. Murray, Modeling sorption of divalent metal cations on hydrous manganese oxide using the diffuse double layer model, *Appl. Geochemistry*, 2004, **19**, 29–53.

8 O. Pourret and M. Davranche, Rare earth element sorption onto hydrous manganese oxide: A modeling study, *J. Colloid Interface Sci.*, 2013, **395**, 18–23.

9 K. Van Sice, C. A. Cravotta, B. McDevitt, T. L. Tasker, J. Landis, J. Puhr and N. R. Warner, Radium attenuation and mobilization in stream sediments following oil and gas wastewater disposal in western Pennsylvania (in press), *Appl. Geochemistry*.

10 F. Carvalho, D. Chambers, S. Fesenko, W. S. Moore, D. Porcelli, H. Vandenhoven and T. Yankovich, *Environmental Pathways and Corresponding Models*, Vienna, 2014.

11 R. B. McCleskey, D. K. Nordstrom, J. N. Ryan and J. W. Ball, A new method of calculating electrical conductivity with applications to natural waters, *Geochim. Cosmochim. Acta*, 2012, **77**, 369–382.

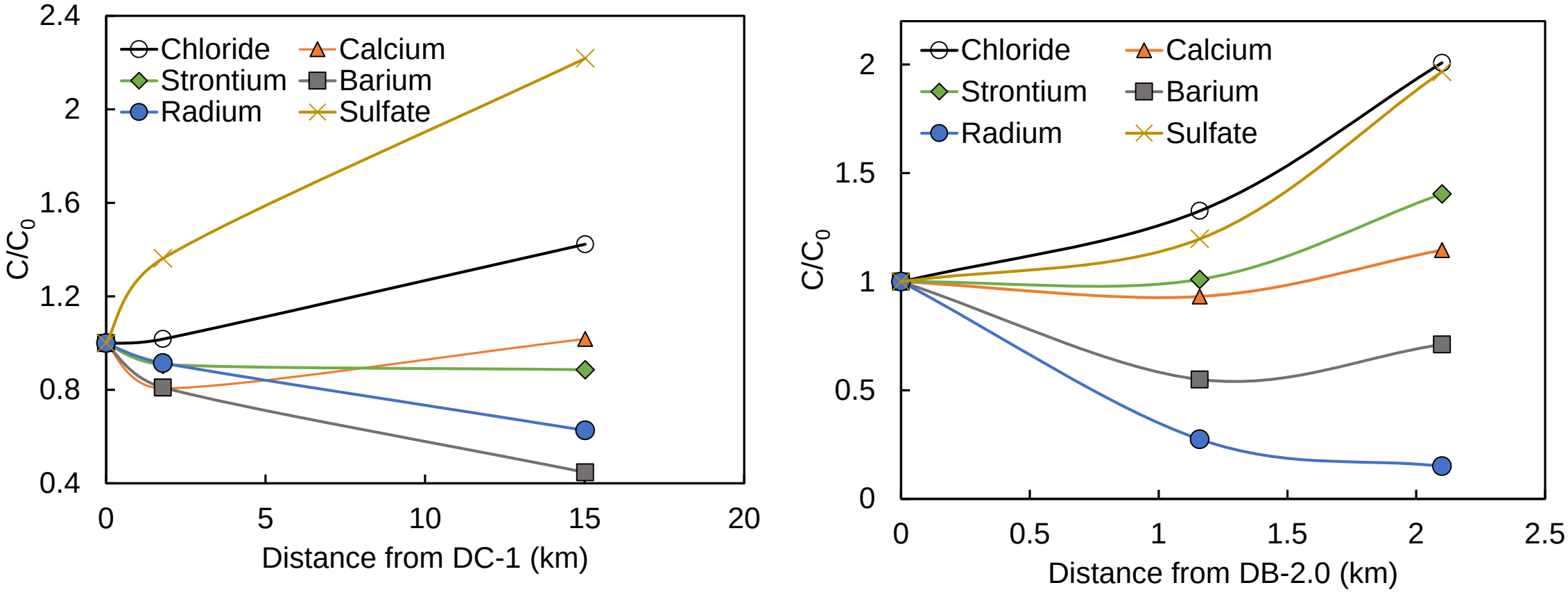


**Figure S1.** Solute concentration factors as a function of evaporation with distance downstream on produced water streams before mixing with lower TDS river waters. Chloride and sodium behaves conservatively while sulfate and cations strontium, calcium, barium and radium do not likely due to mineral precipitation and other geochemical reactions such as ion exchange. Chloride concentration factors were used in PHREEQC model simulations for evaporative extent on produced water streams.

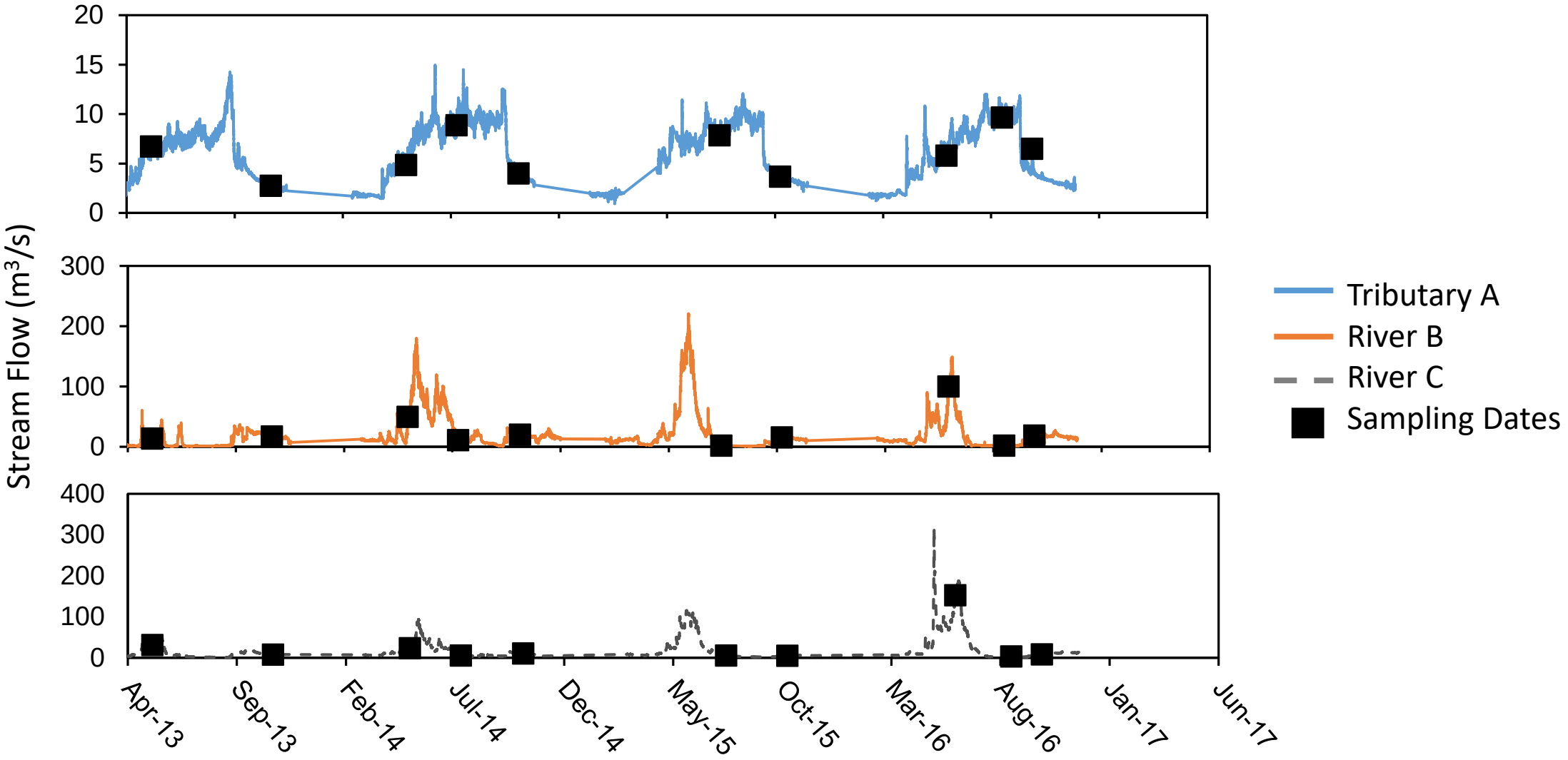


**Figure S2.** Water samples were collected during 10 sampling events between 2013 and 2016 at 28 sites. Sampling occurred in May and November 2013, May, July and October 2014, July and October 2015 and June, August and October 2016. Streamflows in the larger Tributary A and Rivers B and C, determined from USGS stream gauges, indicated relatively constant flows during sampling events except for one potential outlier with peak flows during the June 2016 sampling event likely due to heavy snowmelt not captured during other sampling years.

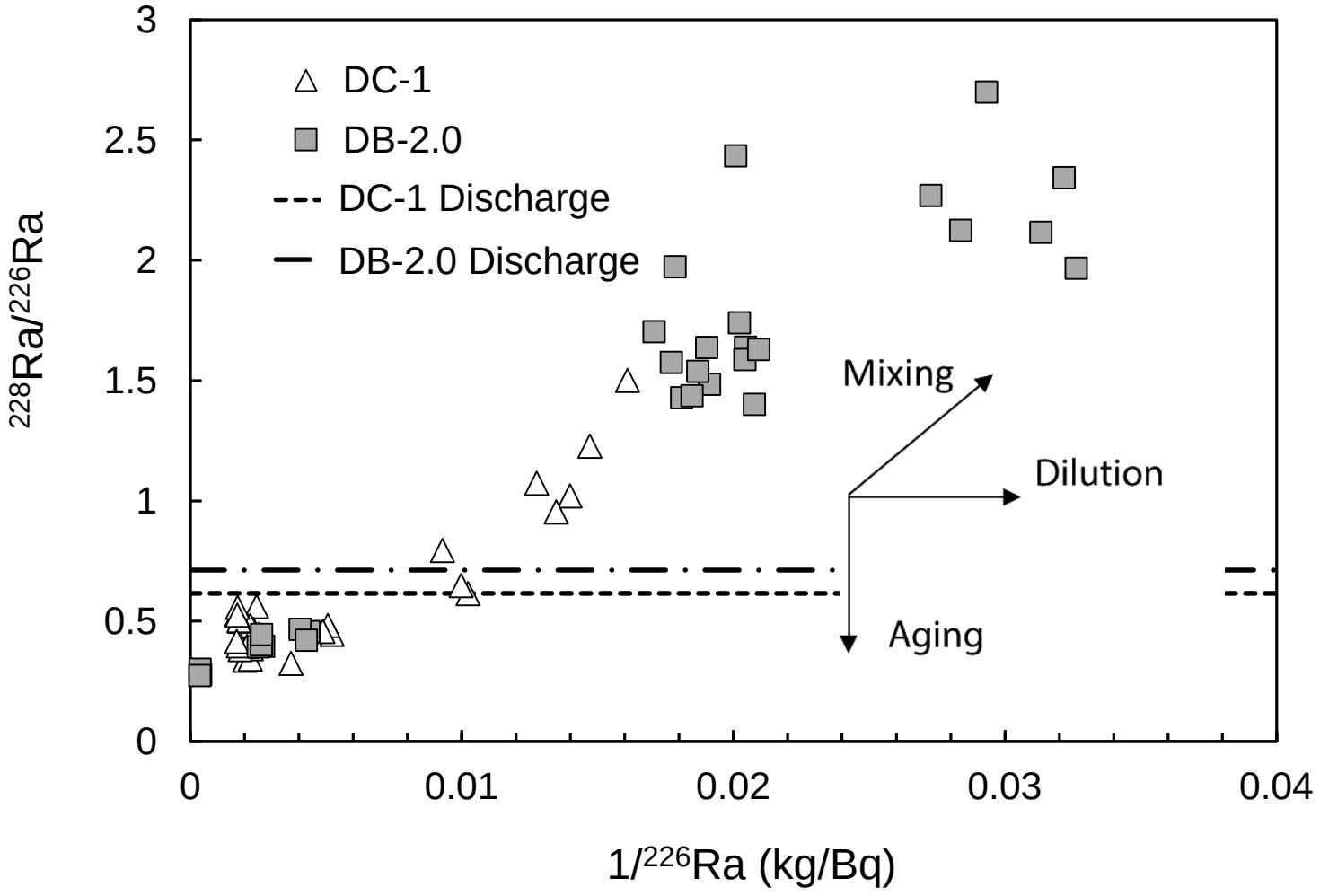


**Figure S3.** Ratios lower than the liquid discharge indicate that some of the radium 228 has decayed and the sediment represents older discharges, while the lower activity samples with higher $^{228}Ra/^{226}Ra$ represent background. Combined the data indicate that radium is present in higher activities at the point of NPDES permitted discharges and mixes with background sediment as the sediments mix downstream.

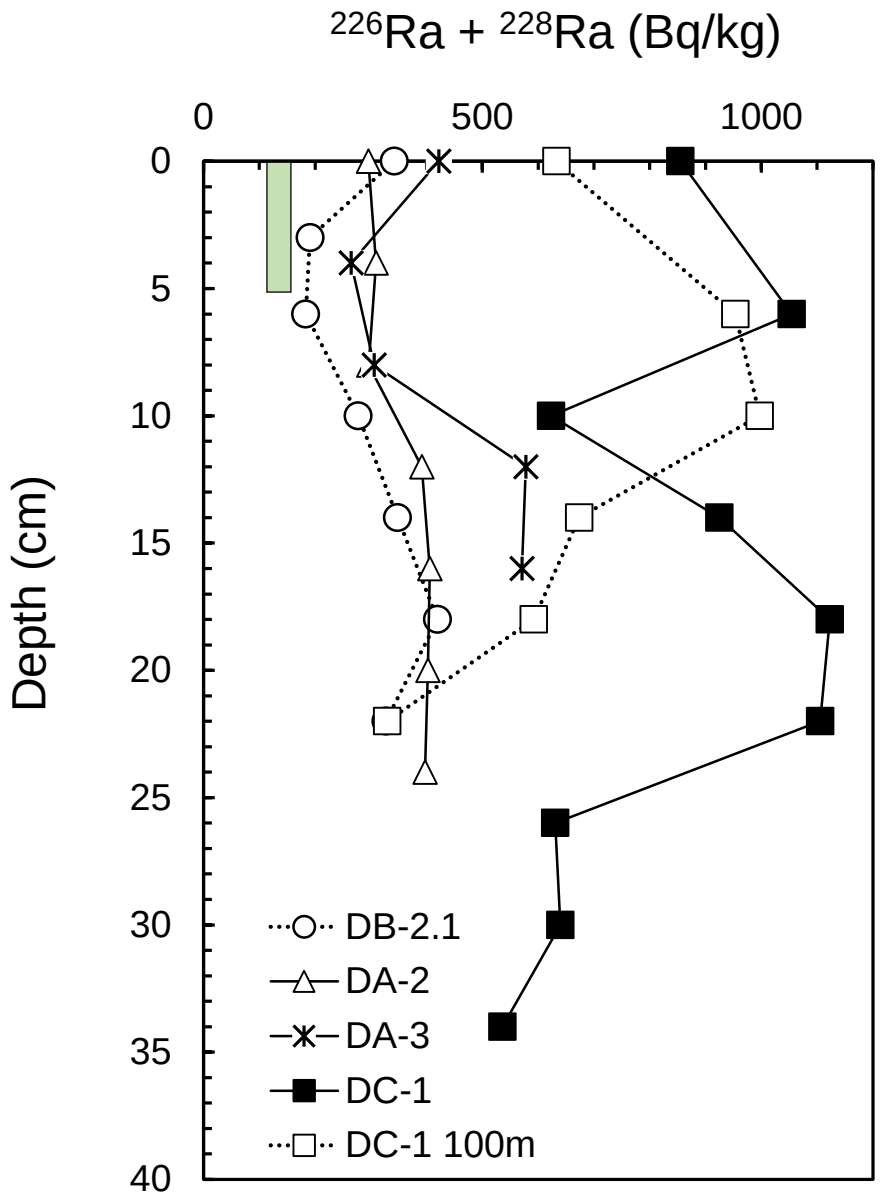


**Figure S4.** Total radium $^{226}Ra + ^{228}Ra$ averages (Bq/kg) versus depth in sediment cores collected near NPDES-permitted discharges DB-2.0, DA-1, DA-2, DA-3, DC-1 and 100 m downstream of DC-1. All cores reflect activities elevated compared to Reference Site grab sediments (105-158 Bq/kg) within the upper 5 cm of soil (green bar).

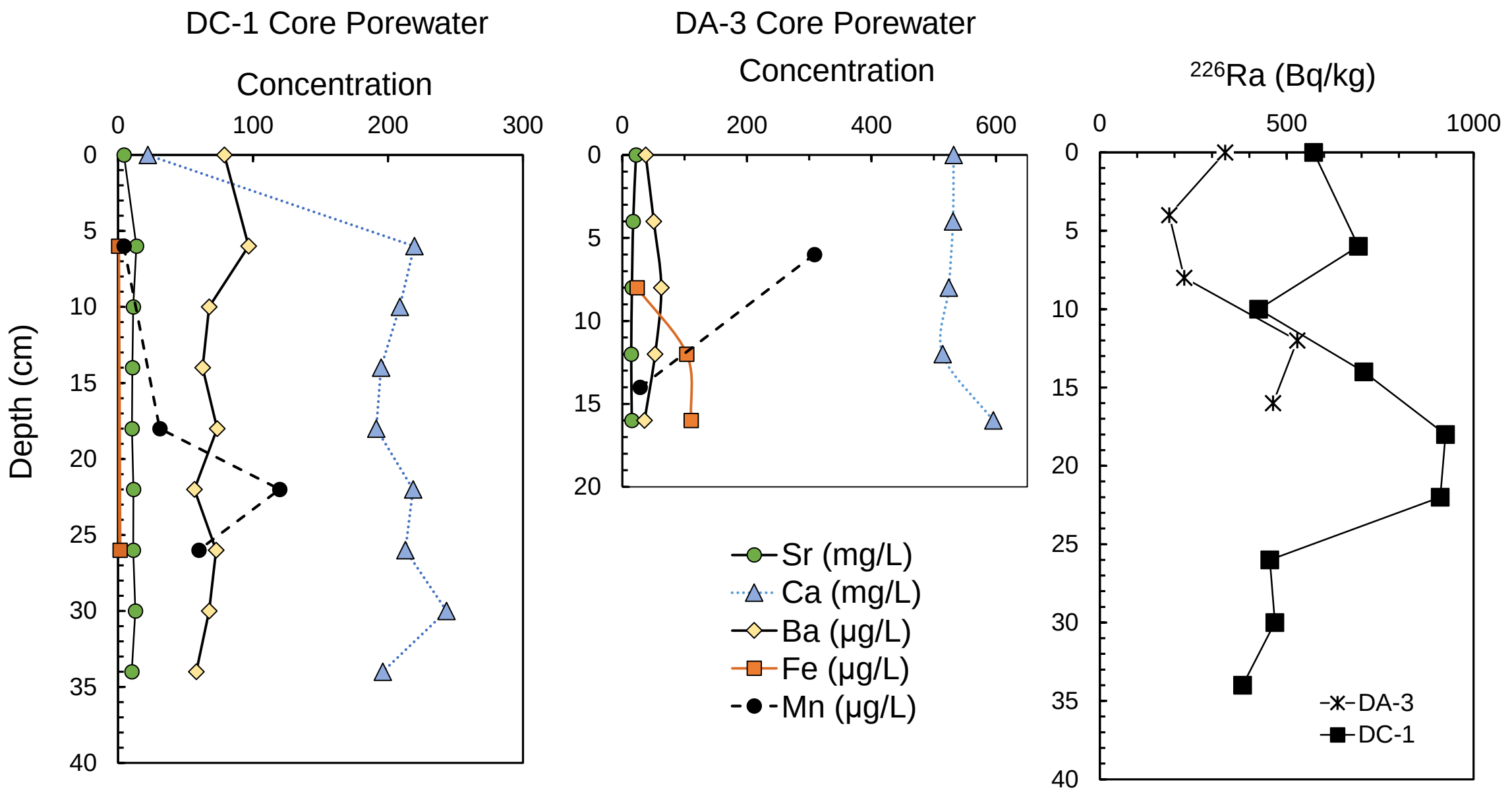


**Figure S5.** DC-1 and DA-3 porewater concentrations for Sr, Ca, Ba, Fe and Mn with depth in the sediment core. A distinct Mn peak of 120 µg/L around 22 cm in depth – coordinated with the $^{226}$Ra peak at the same depth. Iron concentrations were mostly non-detectable. Calcium concentrations remained high throughout the DC-1 core with a small peak around 20 cm in depth and low barium concentrations as much as 3 orders of magnitude less than calcium concentrations in both DC-1 and DA-3 cores.

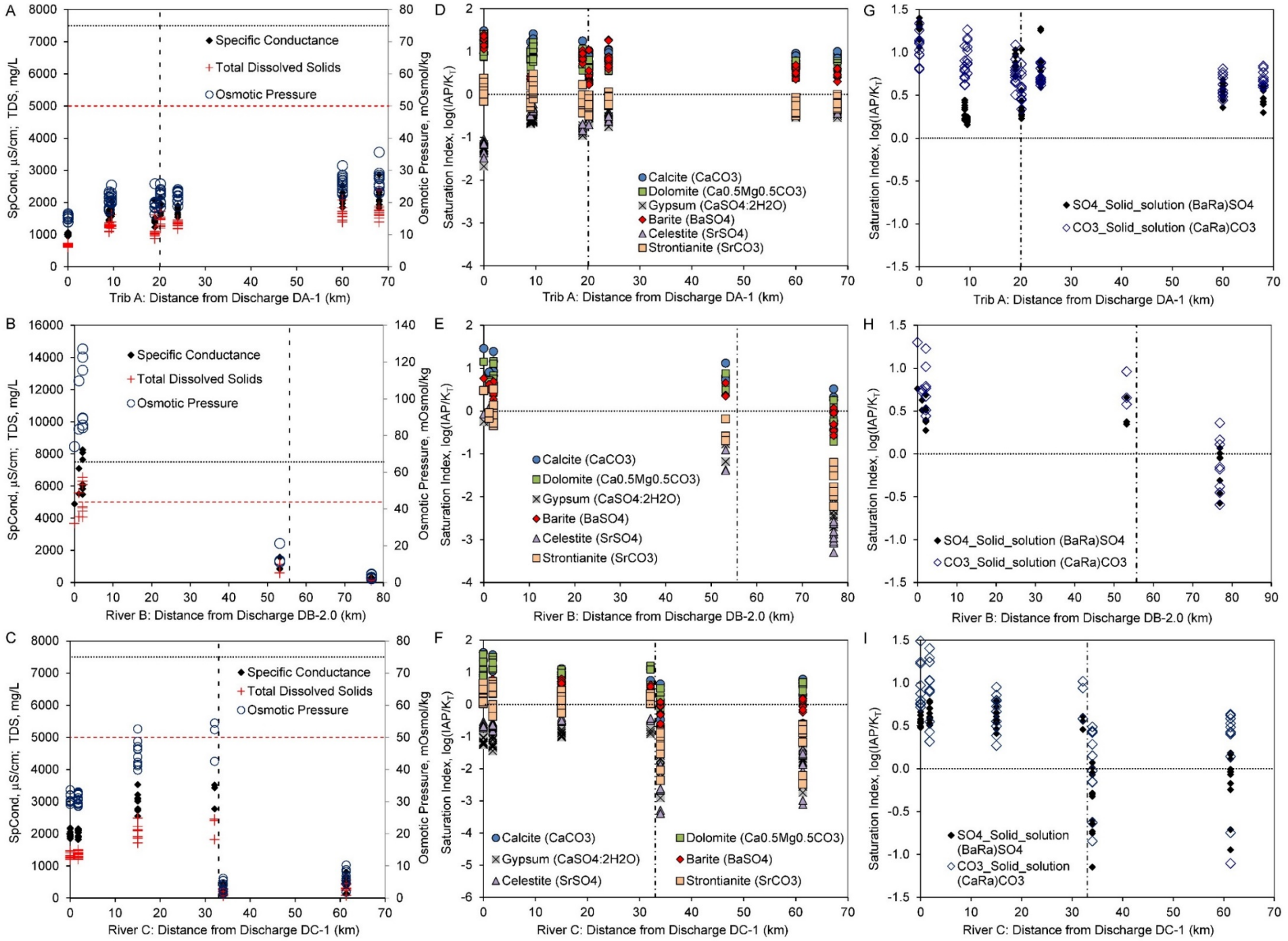


**Figure S6.** TDS, SC, osmotic pressure, and saturation index values computed with PHREEQC for NPDES discharges and selected downstream monitoring sites. Horizontal dashed lines indicate reference conditions for SC = 7,500 mS/cm and OP = 50 mOsmol/kg in A-C, and SI = 0 in D-I. Vertical dashed lines represent confluence points between produced water streams and larger rivers.

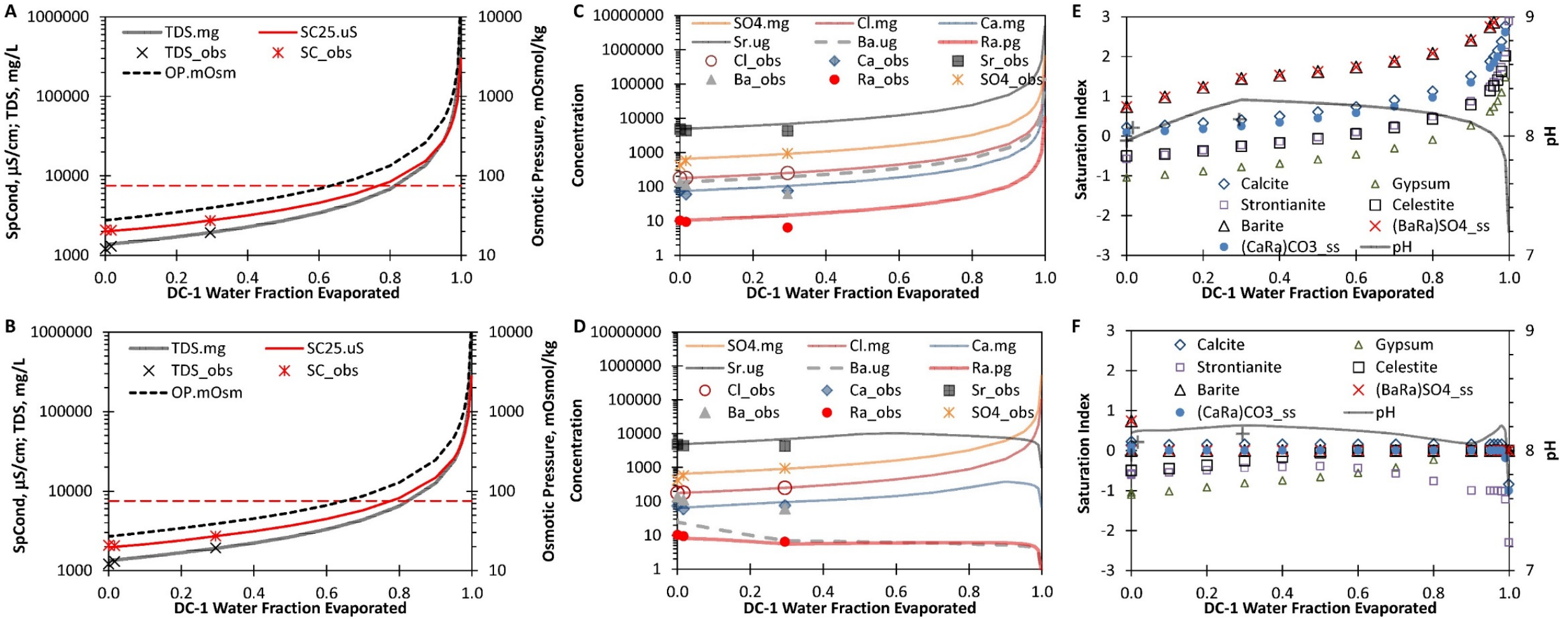


**Figure S7.** PHREEQC simulation of the evaporation of produced water from DB-2.0: (A, C, E) Evaporation without mineral precipitation or adsorption, and (B, D, F) evaporation with precipitation of pure phases and binary solid solutions, (BaRa)$SO_4$ and (CaRa)$CO_3$. (A, B) Simulated total dissolved solids (TDS, mg/L), specific conductance (SC, mS/cm), and osmotic pressure (OP, mOsmol/kg); observed values shown as discrete symbols; dashed line indicates SC of 7,500 mS/cm. (C, D), Simulated aqueous concentrations of sulfate ($SO_4$, mg/L), chloride (Cl, mg/L), calcium (mg/L), barium (Ba, mg/L), strontium (Sr, mg/L), and radium (Ra, pg/L); observed values shown as discrete symbols. (E, F) Simulation results for pH and saturation index (SI) values for selected pure phases and the sulfate and carbonate solid solutions. In B, D, and F, minerals specified to precipitate upon reaching saturation (SI = 0) include gypsum ($CaSO_4$:$2H_2O$), witherite ($BaCO_3$), celestite ($SrSO_4$), strontianite ($SrCO_3$), amorphous ferric hydroxide ($Fe(OH)_3$, "HFO"), and manganite (MnOOH; "HMO"), with dolomite ($Ca_{0.5}Mg_{0.5}CO_3$) specified to precipitate at SI = 0.5. Barite ($BaSO_4$), aragonite ($CaCO_3$), and calcite were not permitted to precipitate when the sulfate and carbonate solid solutions were specified to form. For these simulations of evaporation of DB-2.0, dimensionless Guggenheim mixing parameters of 1.0 were assumed for both solid solutions.

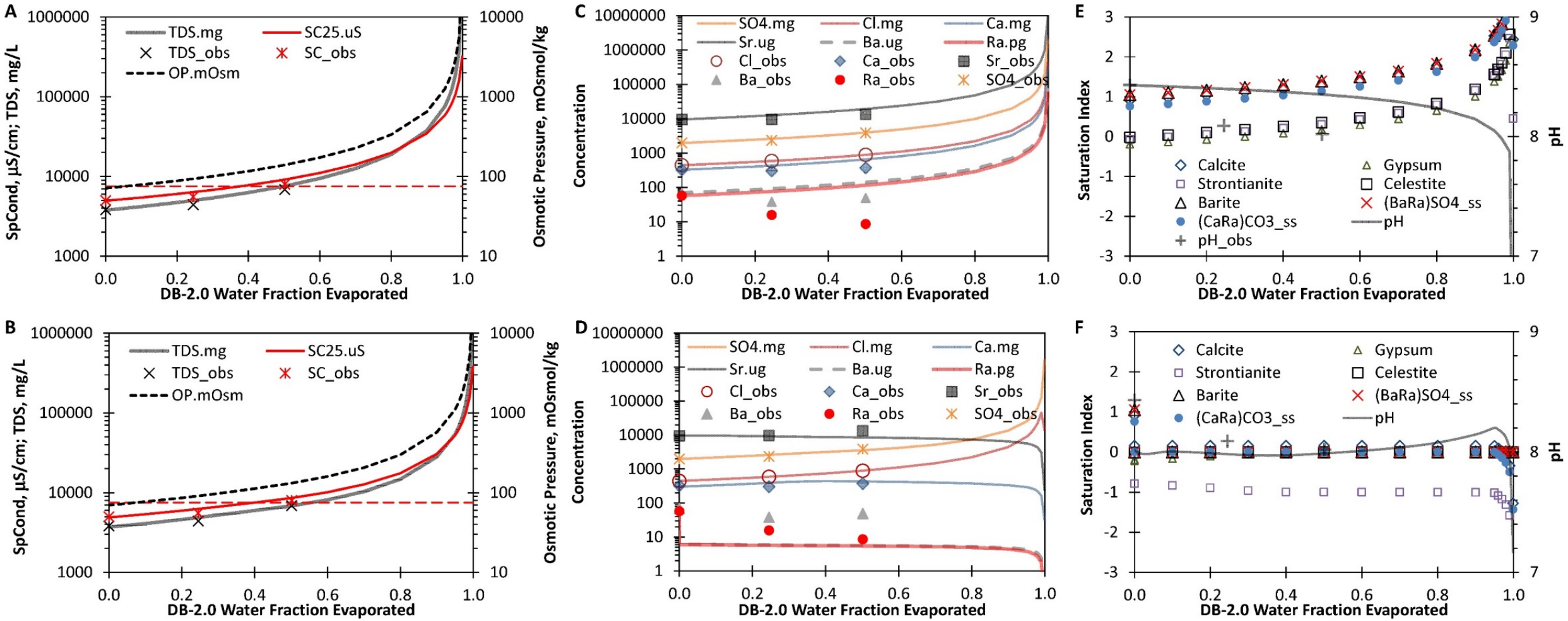
A
SpCond, µS/cm; TDS, mg/L
Osmotic Pressure, mOsmol/kg
TDS.mg
SC25.uS
TDS_obs
SC_obs
OP.mOsm
DB-2.0 Water Fraction Evaporated
B
SpCond, µS/cm; TDS, mg/L
Osmotic Pressure, mOsmol/kg
TDS.mg
SC25.uS
TDS_obs
SC_obs
OP.mOsm
DB-2.0 Water Fraction Evaporated
C
Concentration
SO4.mg
Cl.mg
Ca.mg
Sr.ug
Ba.ug
Ra.pg
Cl_obs
Ca_obs
Sr_obs
Ba_obs
Ra_obs
SO4_obs
DB-2.0 Water Fraction Evaporated
D
Concentration
SO4.mg
Cl.mg
Ca.mg
Sr.ug
Ba.ug
Ra.pg
Cl_obs
Ca_obs
Sr_obs
Ba_obs
Ra_obs
SO4_obs
DB-2.0 Water Fraction Evaporated
E
Saturation Index
pH
Calcite
Strontianite
Barite
(CaRa)CO3_ss
pH_obs
Gypsum
Celestite
(BaRa)SO4_ss
pH
DB-2.0 Water Fraction Evaporated
F
Saturation Index
pH
Calcite
Strontianite
Barite
(CaRa)CO3_ss
Gypsum
Celestite
(BaRa)SO4_ss
pH
DB-2.0 Water Fraction Evaporated

**Figure S8.** PHREEQC simulation of the evaporation of produced water from DC-1: (A, C, E) Evaporation without mineral precipitation or adsorption, and (B, D, F) evaporation with precipitation of pure phases and binary solid solutions, (BaRa)$SO_4$ and (CaRa)$CO_3$. (A, B) Simulated total dissolved solids (TDS, mg/L), specific conductance (SC, μS/cm), and osmotic pressure (OP, mOsmol/kg); observed values shown as discrete symbols; dashed line indicates SC of 7,500 μS/cm. (C, D) Simulated aqueous concentrations of sulfate ($SO_4$, mg/L), chloride (Cl, mg/L), calcium (mg/L), barium (Ba, μg/L), strontium (Sr, μg/L), and radium (Ra, pg/L); observed values shown as discrete symbols. (E, F) Simulation results for pH and saturation index (SI) values for selected pure phases and the sulfate and carbonate solid solutions. In B, D, and F, minerals specified to precipitate upon reaching saturation (SI = 0) include gypsum ($CaSO_4$:$2H_2O$), witherite ($BaCO_3$), celestite ($SrSO_4$), strontianite ($SrCO_3$), amorphous ferric hydroxide ($Fe(OH)_3$, “HFO”), and manganite (MnOOH; “HMO”), with dolomite ($Ca_{0.5}Mg_{0.5}CO_3$) specified to precipitate at SI = 0.5. Barite ($BaSO_4$), aragonite ($CaCO_3$), and calcite were not permitted to precipitate when the sulfate and carbonate solid solutions were specified to form. For these simulations of evaporation of DC-1, dimensionless Guggenheim mixing parameter of 1.0 was assumed for (CaRa)$CO_3$ and 3.5 for (BaRa)$SO_4$.

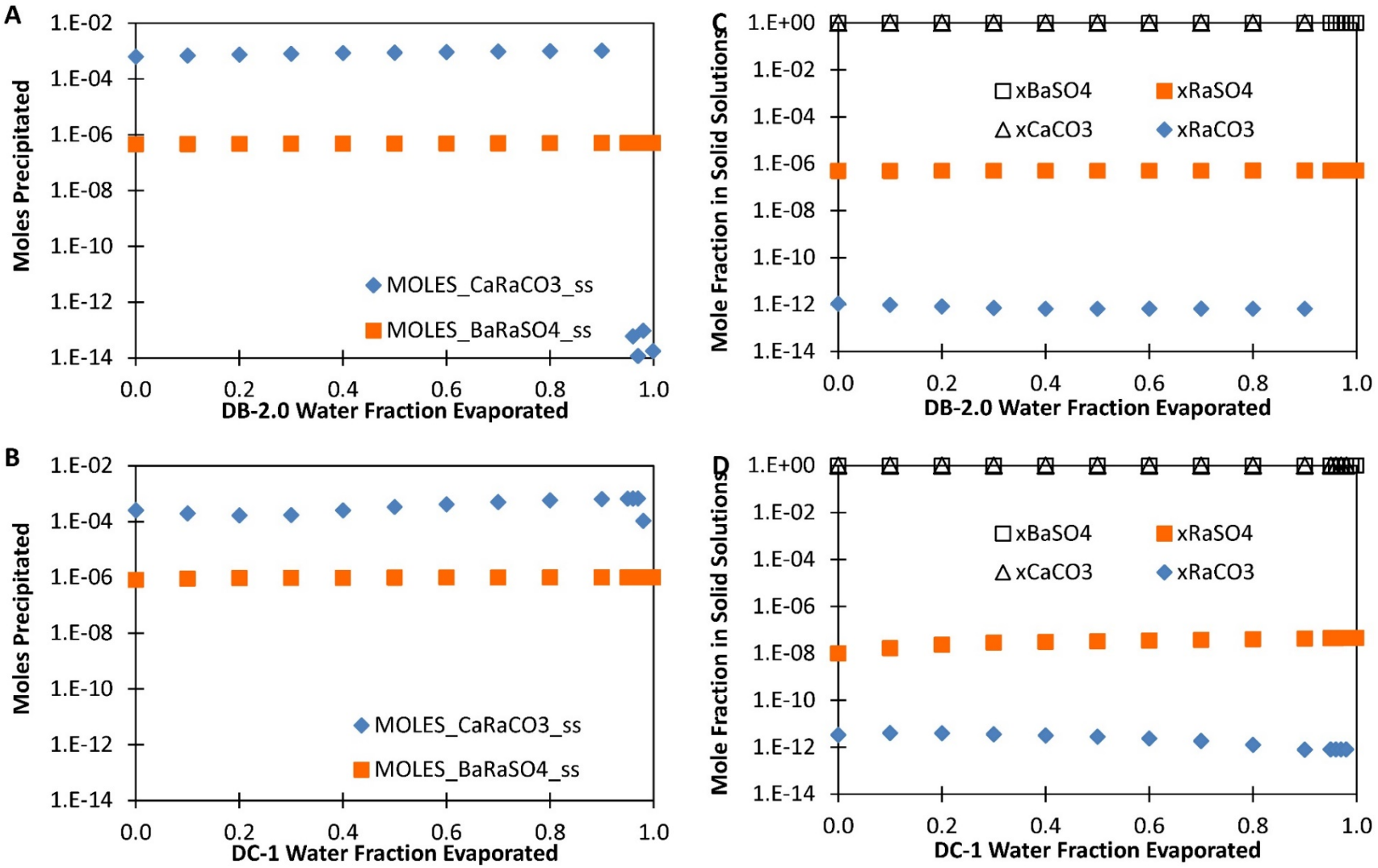


**Figure S9.** PHREEQC simulated evaporation of produced water from (A, C) DB 2.0 and (B, D) DC-1: (A, B) Moles of (Ca,Ra)$CO_3$ and (Ba,Ra)$SO_4$ precipitated, and (C, D) corresponding mole fractions of components in the solid solutions. Dimensionless Guggenheim mixing parameter of 1.0 for both (Ca,Ra)$CO_3$ and (Ba,Ra)$SO_4$ was assumed for simulations of DB-2.0; mixing parameter values of 1.0 for (Ca,Ra)$CO_3$ and 3.5 for (Ba,Ra)$SO_4$ were assumed for simulations of DC-1.

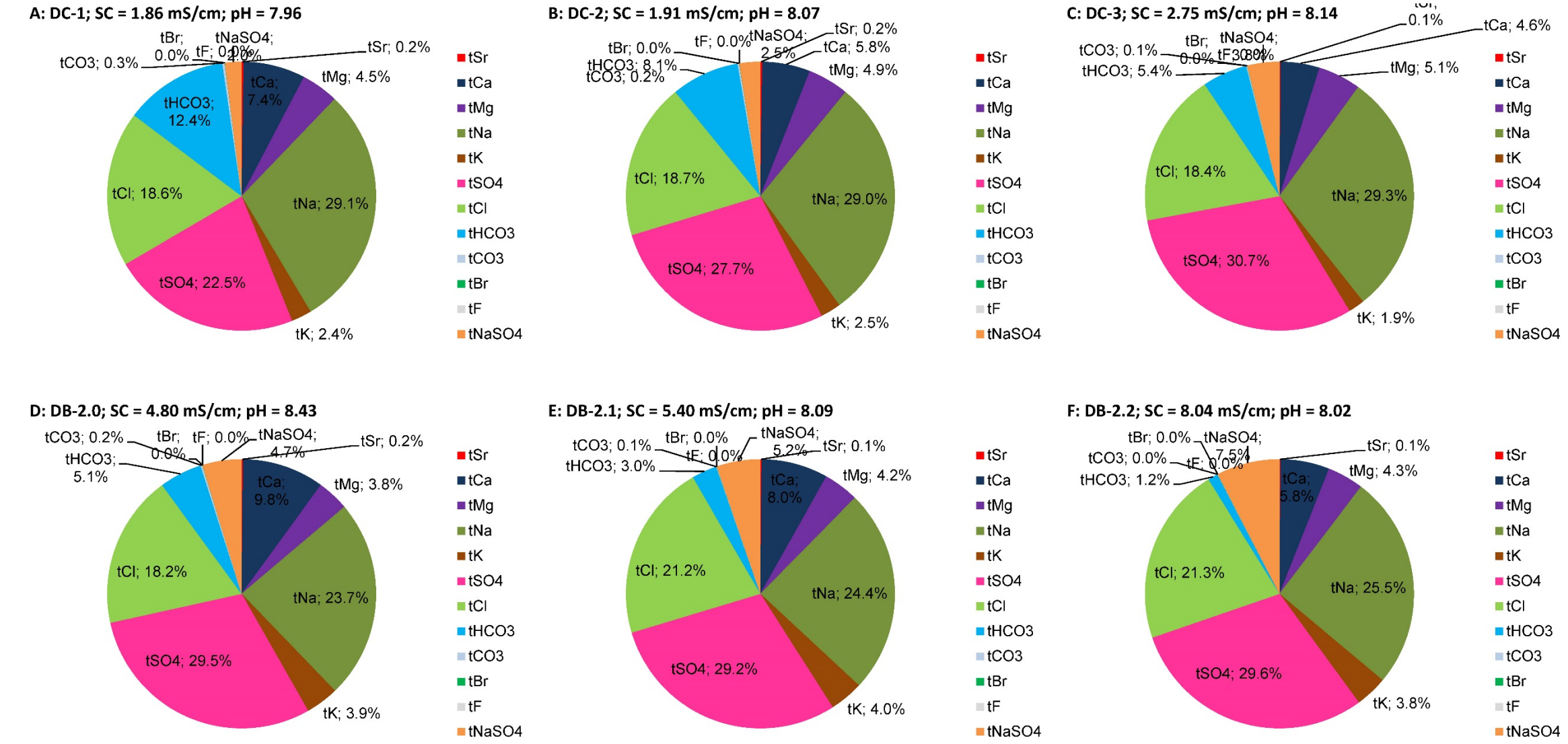


**Figure S10.** Major ion contributions to specific conductance (SC) for selected NPDES-permitted discharges and downstream water samples. Values are the estimated contributions by major ion species to computed SC, expressed in percent, October 2016. Individual ion conductivities estimated from dissolved constituent concentrations as the transport number (relative contribution of a given ion to the overall conductivity, using the methods of McCleskey and others (2012) after aqueous speciation calculations with PHREEQC (Parkhurst and Appelo, 2013). Temperature correction of 2% per degree C applied to computed SC.

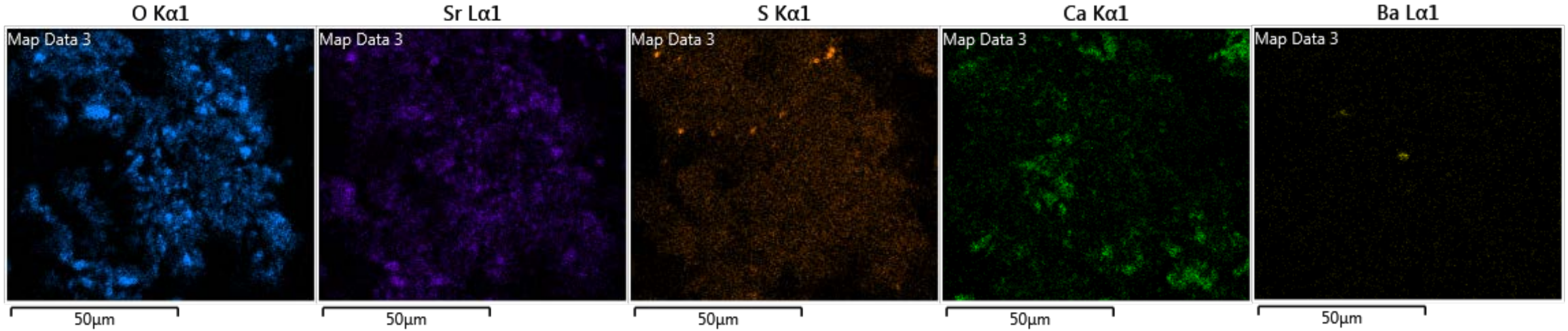


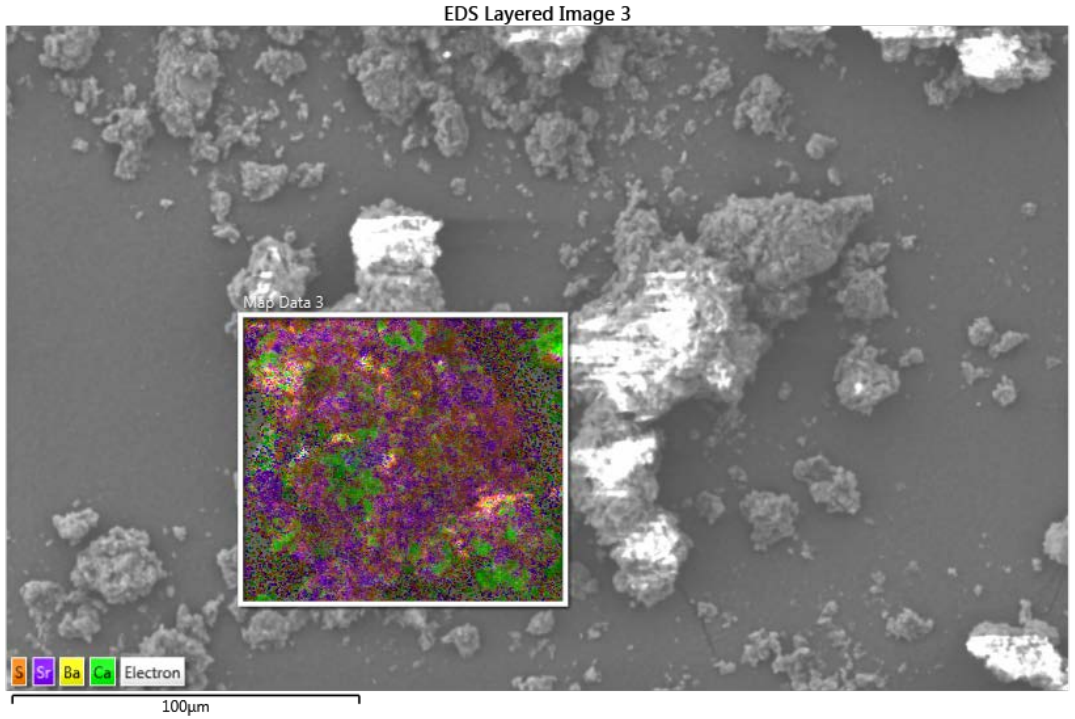


**Figure S11.** EDS images of DC-1 leach step 4 residue (post-HCl application). Sr, S and Ca overlay in the image while very little Ba is present.

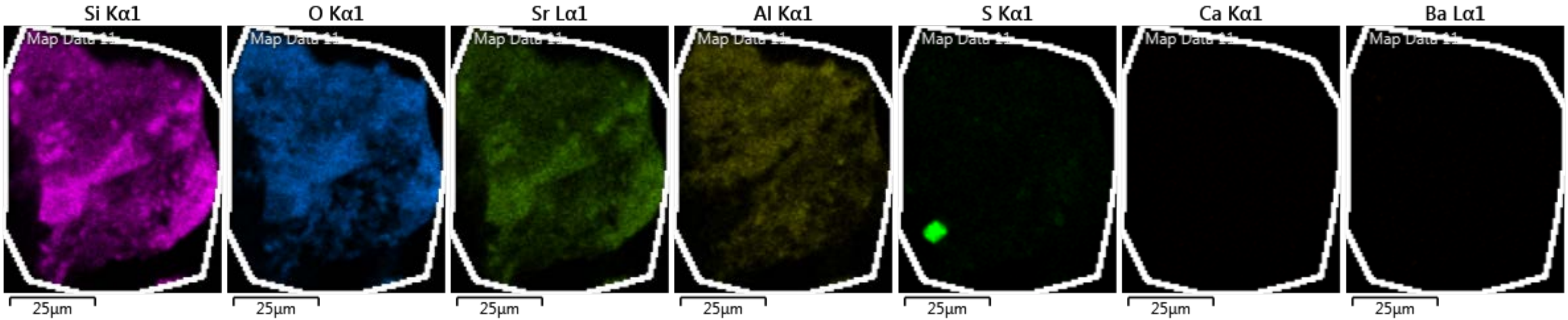


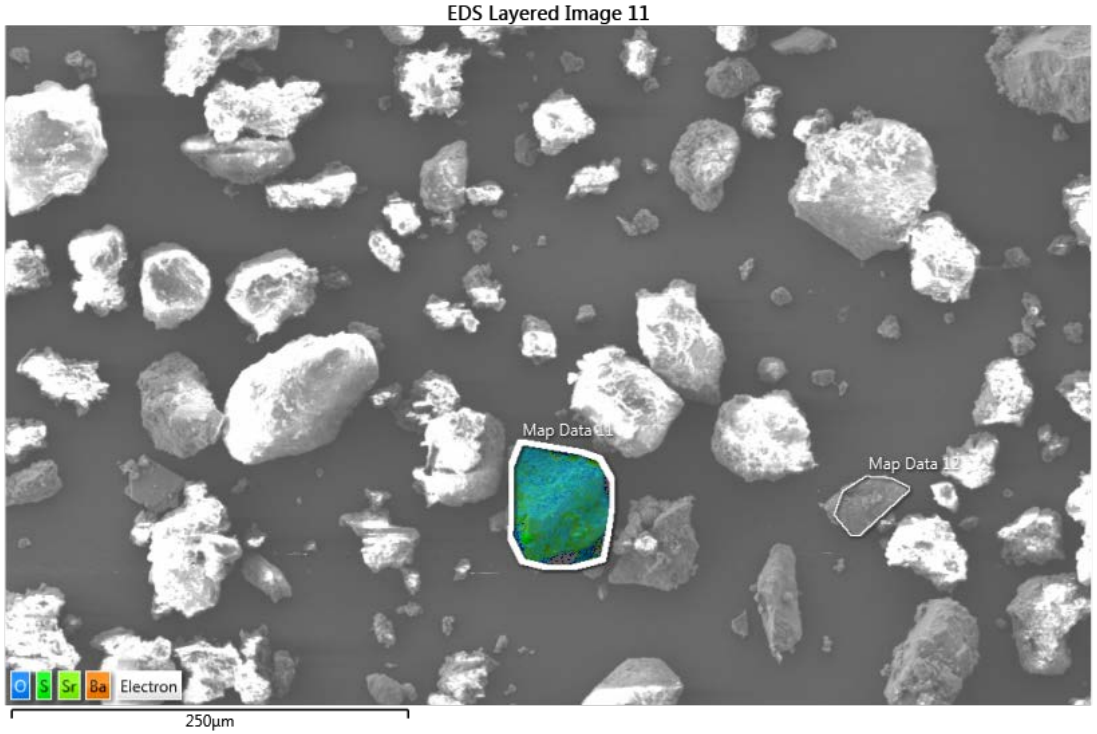


**Figure S12.** EDS images of DB-2.0 leach step 4 residue (post-HCl application). Sr is present though does not overlay with S and no Ba was detected. Typical clay elements Al and Si were visible.

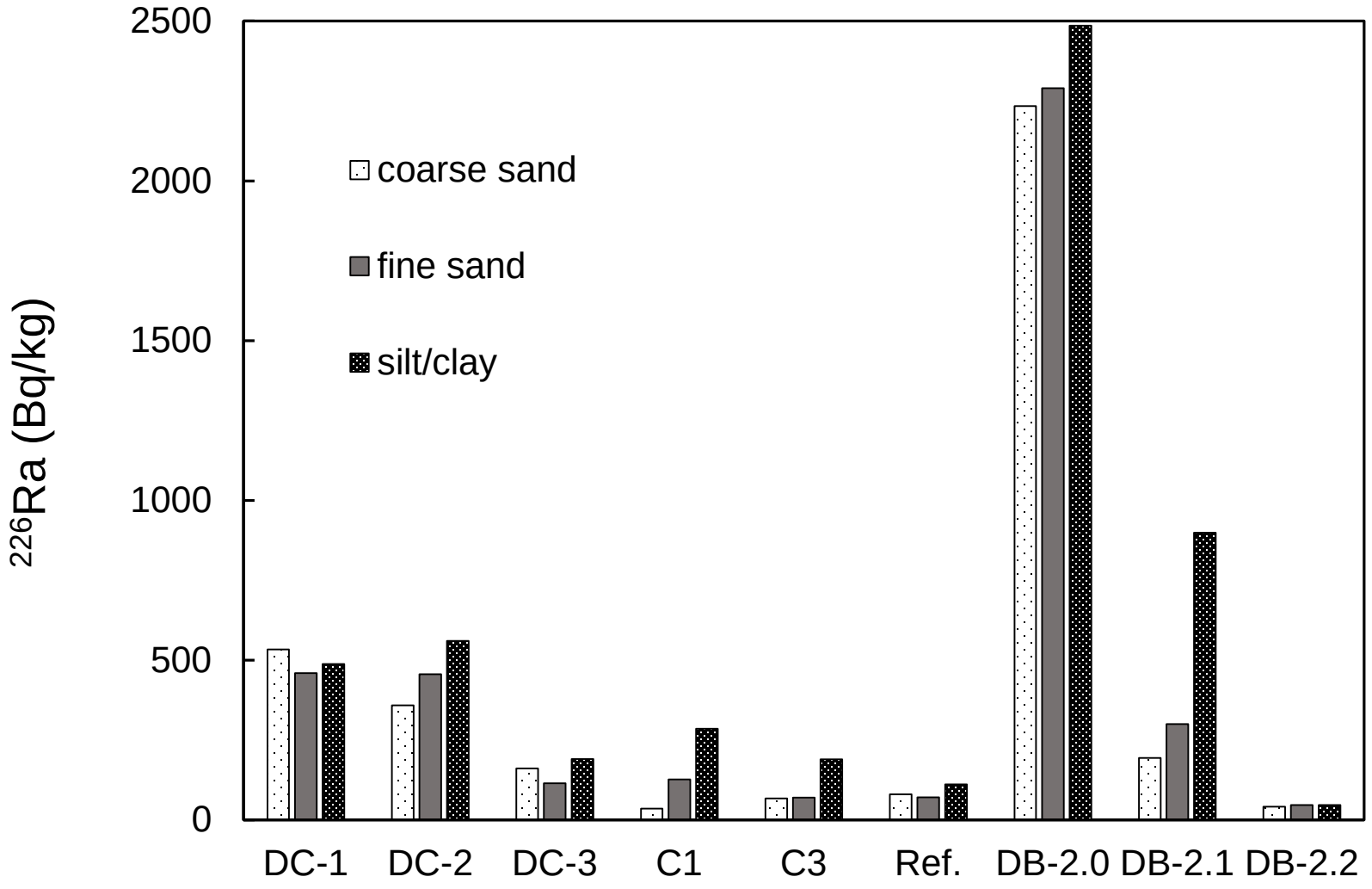


**Figure S13.** Radium 226 activity in sediment samples separated based on size fractions. Note that at discharge sites DC-1, DB-2.0, and to a lesser extent DC-2, regardless of grain-size the radium activity at each sample site is similar. In contrast, the background sediment at the reference site as well as C1 and C3 contain higher relative activity in the smaller grain size fraction.

**Table S1**. Sampling data averages ± standard deviation (SD) for each of the 28 sites sampled between 2013-2016 including field parameters, major cations and anions, water types, and radium activities in the water and in the sediment.

| Site Name* | pH (su) | Temperature (°C) | Electrical Conductivity (µS/cm) | Dissolved Oxygen (mg/L) | TDS (mg/L) | Chloride (mg/L) | Sulfate (mg/L) | Alkalinity (mg/L) | Fluoride (mg/L) | Calcium (mg/L) | Barium (mg/L) | Strontium (mg/L) | Sodium (mg/L) | Magnesium (mg/L) | Potassium (mg/L) | Iron** (µg/L) | Manganese (µg/L) | Water type | $^{226}$Ra (pCi/L) | $^{226}$Ra (Bq/L) | $^{228}$Ra** (pCi/L) | $^{228}$Ra** (Bq/L) | $^{226}$Ra+$^{228}$Ra (Bq/L) | $^{226}$Ra (Bq/kg) | $^{228}$Ra (Bq/kg) | $^{226}$Ra+$^{228}$Ra (Bq/kg) | $^{226}$Ra+$^{228}$Ra (pCi/g) | Fails to meet sediment action level for $^{226}$Ra | # samples dissolved | # samples sediment |
|---|---|---|---|---|---|---|---|---|---|---|---|---|---|---|---|---|---|---|---|---|---|---|---|---|---|---|---|---|---|---|
| A1 | 7.9 ± 0.2 | 12 ± 5 | 1889 ± 183 | 8.41 ± 1.22 | 1408 ± 193 | 30 ± 3 | 875 ± 125 | 226 ± 56 | 1.9 ± 0.3 | 241 ± 35 | 0.05 ± 0.04 | 6.8 ± 1.3 | 105 ± 22 | 65 ± 5 | 11 ± 1 | 175 ± 86 | 28 ± 10 | calcium-sulfate | 1.91 ± 0.29 | 0.07 ± 0.01 | 2.34 | 0.09 | 0.16 | 76 ± 18 | 57 ± 9 | 134 | 3.6 | | 11 | 6 |
| A2 | 8.1 ± 0.2 | 12 ± 5 | 1759 ± 92 | 8.80 ± 1.04 | 1271 ± 120 | 29 ± 3 | 759 ± 71 | 255 ± 57 | 1.6 ± 0.4 | 191 ± 36 | 0.11 ± 0.07 | 5.0 ± 0.9 | 129 ± 45 | 60 ± 10 | 11 ± 1 | nd | 94 ± 43 | calcium-sulfate | 1.29 ± 0.58 | 0.05 ± 0.02 | nd | nd | 0.05 | 68 ± 4 | 49 ± 15 | 117 | 3.2 | | 11 | 7 |
| A3 | 8.0 ± 0.1 | 11 ± 6 | 2133 ± 184 | 9.12 ± 1.27 | 1621 ± 209 | 34 ± 4 | 1019 ± 144 | 250 ± 52 | 1.5 ± 0.1 | 247 ± 28 | 0.05 ± 0.01 | 6.2 ± 0.5 | 148 ± 21 | 78 ± 7 | 11 ± 1 | nd | 123 ± 82 | calcium-sulfate | nd | nd | nd | nd | nd | 41 ± 5 | 56 ± 11 | 97 | 2.6 | | 11 | 7 |
| A4 | 8.1 ± 0.1 | 12 ± 6 | 2224 ± 267 | 9.16 ± 1.15 | 1730 ± 303 | 35 ± 5 | 1103 ± 223 | 225 ± 40 | 1.4 ± 0.2 | 251 ± 31 | 0.04 ± 0.01 | 6.3 ± 0.6 | 164 ± 38 | 81 ± 11 | 11 ± 1 | nd | 37 ± 16 | calcium-sulfate | 0.21 ± 0.10 | 0.01 ± 0.00 | 1.13 | 0.04 | 0.05 | 31 ± 4 | 36 ± 7 | 67 | 1.8 | | 10 | 7 |
| DA-1 | 8.3 ± 0.1 | 20 ± 3 | 1051 ± 40 | 6.45 ± 0.47 | 528 ± 95 | 25 ± 3 | 127 ± 28 | 414 ± 60 | 2.1 ± 0.4 | 104 ± 9 | 0.76 ± 0.10 | 2.7 ± 0.1 | 59 ± 7 | 44 ± 1 | 11 ± 1 | nd | 6 ± 3 | calcium-magnesium-bicarbonate | 4.98 ± 0.74 | 0.18 ± 0.03 | 1.31 | 0.05 | 0.23 | 238 ± 58 | 77 ± 17 | 315 | 8.5 | x | 11 | 5 |
| DA-2 | 7.9 ± 0.1 | 20 ± 3 | 1599 ± 243 | 6.61 ± 0.76 | 1172 ± 104 | 27 ± 3 | 663 ± 71 | 303 ± 47 | 2.2 ± 0.1 | 214 ± 11 | 0.04 ± 0.01 | 6.1 ± 0.3 | 85 ± 22 | 56 ± 3 | 10 ± 1 | nd | 36 ± 8 | calcium-sulfate | 4.04 ± 0.56 | 0.15 ± 0.02 | 1.18 | 0.04 | 0.19 | 237 ± 11 | 63 ± 3 | 300 | 8.1 | x | 11 | 7 |
| DA-3 | 8.0 ± 0.1 | 22 ± 2 | 1765 ± 119 | 6.25 ± 0.55 | 1234 ± 235 | 34 ± 4 | 676 ± 184 | 367 ± 66 | 2.4 ± 0.3 | 245 ± 11 | 0.04 ± 0.00 | 9.0 ± 0.2 | 61 ± 18 | 67 ± 6 | 14 ± 1 | nd | 4 ± 1 | calcium-sulfate | 9.03 ± 2.66 | 0.33 ± 0.10 | 1.40 | 0.05 | 0.39 | 483 ± 173 | 100 ± 20 | 583 | 15.7 | x | 11 | 7 |
| DA-4 | 8.1 ± 0.2 | 13 ± 5 | 1493 ± 197 | 8.74 ± 1.09 | 994 ± 191 | 28 ± 3 | 518 ± 156 | 326 ± 51 | 1.8 ± 0.1 | 153 ± 42 | 0.14 ± 0.03 | 3.7 ± 1.0 | 100 ± 13 | 60 ± 3 | 11 ± 1 | nd | 84 ± 63 | calcium-magnesium-sulfate-bicarbonate | 0.92 ± 1.10 | 0.03 ± 0.04 | 2.63 | 0.10 | 0.13 | 83 ± 29 | 57 ± 7 | 141 | 3.8 | | 10 | 11 |
| B1 | 8.2 ± 0.3 | 12 ± 3 | 190 ± 63 | 9.40 ± 0.45 | 98 ± 34 | 2 ± 1 | 16 ± 8 | 85 ± 29 | 0.2 ± 0.0 | 23 ± 8 | 0.08 ± 0.06 | 0.1 ± 0.0 | 7 ± 2 | 6 ± 3 | 2 ± 0 | 143 ± 35 | 7 ± 4 | calcium-bicarbonate | 0.26 ± 0.11 | 0.01 ± 0.00 | nd | nd | 0.01 | 54 ± 19 | 362 ± 308 | 415 | 11.2 | | 8 | 7 |
| B2 | 8.3 ± 0.2 | 14 ± 5 | 207 ± 62 | 8.92 ± 0.77 | 106 ± 34 | 2 ± 1 | 21 ± 8 | 85 ± 28 | 0.2 ± 0.1 | 25 ± 8 | 0.07 ± 0.04 | 0.1 ± 0.0 | 8 ± 2 | 7 ± 3 | 2 ± 0 | 139 ± - | 6 ± 1 | calcium-bicarbonate | 0.27 ± 0.19 | 0.01 ± 0.01 | nd | nd | 0.01 | 30 ± 7 | 67 ± 19 | 98 | 2.6 | | 8 | 7 |
| B3 | 8.2 ± 0.3 | 12 ± 5 | 231 ± 69 | 9.04 ± 1.23 | 107 ± 38 | 2 ± 1 | 24 ± 9 | 97 ± 34 | 0.2 ± 0.0 | 27 ± 8 | 0.05 ± 0.02 | 0.2 ± 0.0 | 9 ± 2 | 7 ± 3 | 2 ± 0 | nd | 6 ± 2 | calcium-bicarbonate | 0.27 ± 0.16 | 0.01 ± 0.01 | 1.17 | 0.04 | 0.05 | 44 ± 6 | 137 ± 18 | 181 | 4.9 | | 10 | 7 |
| UDB-1.0 | 8.5 ± 0.3 | 16 ± 6 | 712 ± 249 | 8.46 ± 1.25 | 446 ± 179 | 2 ± 1 | 215 ± 102 | 168 ± 47 | 0.2 ± 0.0 | 84 ± 31 | 0.07 ± 0.02 | 1.1 ± 0.5 | 43 ± 17 | 19 ± 7 | 2 ± 1 | nd | 54 ± 40 | calcium-sulfate | 0.33 ± 0.10 | 0.01 ± 0.00 | nd | nd | 0.01 | 40 ± 3 | 54 ± 7 | 94 | 2.5 | | 5 | 7 |
| DB-1.0 | 8.3 ± 0.3 | 11 ± 10 | 9820 ± 3321 | 5.80 ± 1.65 | 6709 ± 3052 | 1673 ± 510 | 2183 ± 1696 | 1365 ± 895 | 4.1 ± 2.7 | 149 ± 94 | 0.16 ± 0.08 | 7.5 ± 2.8 | 2157 ± 629 | 166 ± 163 | 20 ± 8 | 133 ± 35 | 80 ± 40 | sodium-chloride | 0.18 ± 0.10 | 0.01 ± 0.00 | 1.14 | 0.04 | 0.05 | 55 ± 6 | 53 ± 6 | 108 | 2.9 | | 3 | 4 |
| DB-1.1 | 8.4 ± 0.2 | 17 ± 6 | 738 ± 260 | 8.23 ± 1.20 | 459 ± 190 | 13 ± 8 | 202 ± 104 | 177 ± 39 | 0.2 ± 0.1 | 71 ± 24 | 0.06 ± 0.01 | 0.9 ± 0.3 | 67 ± 30 | 17 ± 7 | 2 ± 1 | nd | 7 ± 6 | calcium-sodium-sulfate-bicarbonate | 0.32 ± 0.27 | 0.01 ± 0.01 | 1.40 | 0.05 | 0.06 | 44 ± 3 | 78 ± 10 | 122 | 3.3 | | 8 | 7 |
| DB-2.0* | 8.4 ± - | 8 ± - | 4983 ± - | 1.15 ± - | 3822 ± - | 440 ± - | 1958 ± - | 471 ± - | no value | 323 ± - | 0.07 ± - | 9.5 ± - | 684 ± - | 76 ± - | 111 ± - | nd | 9 ± - | sodium-sulfate | 33.40 ± - | 1.24 ± - | 23.80 | 0.88 | 2.12 | 2690 ± 130 | 763 ± 50 | 3453 | 93.3 | x | 1 | 3 |
| DB-2.1 | 7.9 ± 0.2 | 14 ± 7 | 6583 ± 1462 | 8.87 ± 1.65 | 5089 ± 965 | 660 ± 109 | 2697 ± 499 | 331 ± 40 | no value | 359 ± 81 | 0.05 ± 0.02 | 11.1 ± 2.1 | 947 ± 203 | 117 ± 27 | 148 ± - | nd | 84 ± 91 | sodium-sulfate | 12.95 ± 2.76 | 0.48 ± 0.10 | 5.85 | 0.22 | 0.70 | 309 ± 79 | 68 ± 28 | 378 | 10.2 | x | 2 | 7 |
| DB-2.2 | 8.3 ± 0.1 | 15 ± 9 | 6565 ± 1200 | 8.84 ± 1.88 | 5264 ± 1164 | 632 ± 156 | 2860 ± 701 | 235 ± 193 | 3.0 ± 0.3 | 348 ± 37 | 0.04 ± 0.01 | 12.1 ± 1.6 | 1025 ± 239 | 146 ± 21 | 181 ± 34 | nd | 14 ± 10 | sodium-sulfate | 8.93 ± 1.77 | 0.33 ± 0.07 | 2.42 | 0.09 | 0.42 | 51 ± 4 | 89 ± 20 | 139 | 3.8 | | 7 | 7 |
| DB-3 | 8.3 ± 0.2 | 14 ± 4 | 1080 ± 376 | 8.13 ± 0.67 | 754 ± 333 | 19 ± 12 | 389 ± 210 | 221 ± 30 | 0.2 ± 0.1 | 104 ± 29 | 0.06 ± 0.01 | 1.4 ± 0.5 | 102 ± 56 | 29 ± 12 | 3 ± 1 | nd | 9 ± 6 | calcium-sodium-sulfate | 0.48 ± 0.14 | 0.02 ± 0.01 | nd | nd | 0.02 | 53 ± 2 | 83 ± 5 | 136 | 3.7 | | 3 | 7 |
| DB-4.0 | 8.0 ± 0.3 | 12 ± 7 | 7833 ± 1094 | 9.07 ± 3.25 | 5693 ± 874 | 962 ± 207 | 2750 ± 382 | 1147 ± 406 | 3.4 ± 0.7 | 280 ± 49 | 0.04 ± 0.01 | 10.7 ± 1.2 | 1413 ± 201 | 110 ± 14 | 148 ± 22 | nd | 4 ± 2 | sodium-sulfate-chloride | 4.56 ± 1.28 | 0.17 ± 0.05 | 3.30 | 0.12 | 0.29 | 99 ± 3 | 111 ± 3 | 210 | 5.7 | | 3 | 4 |
| DB-4.1 | 7.9 ± 0.2 | 14 ± 5 | 2186 ± 597 | 8.91 ± 1.70 | 1641 ± 884 | 194 ± 158 | 866 ± 598 | 265 ± 69 | 0.6 ± 0.2 | 188 ± 38 | 0.05 ± 0.01 | 2.3 ± 0.8 | 227 ± 97 | 60 ± 16 | 9 ± 5 | nd | 56 ± 28 | sodium-calcium-sulfate | 0.25 ± 0.07 | 0.01 ± 0.00 | 1.07 | 0.04 | 0.05 | 42 ± 14 | 83 ± 28 | 125 | 3.4 | | 10 | 6 |
| C1 | 8.4 ± 0.2 | 15 ± 5 | 264 ± 131 | 8.61 ± 1.02 | 139 ± 79 | 3 ± 2 | 51 ± 35 | 84 ± 34 | 0.2 ± 0.0 | 30 ± 14 | 0.04 ± 0.03 | 0.3 ± 0.2 | 10 ± 5 | 9 ± 5 | 1 ± 1 | 103 ± 3 | 9 ± 2 | calcium-bicarbonate-sulfate | 0.86 ± 0.35 | 0.03 ± 0.01 | nd | nd | 0.03 | 36 ± 7 | 35 ± 5 | 71 | 1.9 | | 13 | 7 |
| C2 | 8.4 ± 0.2 | 15 ± 6 | 271 ± 131 | 8.92 ± 1.05 | 144 ± 81 | 3 ± 2 | 52 ± 37 | 86 ± 36 | 0.2 ± 0.0 | 31 ± 14 | 0.03 ± 0.02 | 0.3 ± 0.2 | 10 ± 6 | 10 ± 5 | 1 ± 1 | nd | 9 ± 2 | calcium-bicarbonate-sulfate | 0.79 ± 0.31 | 0.03 ± 0.01 | nd | nd | 0.03 | 62 ± 10 | 64 ± 13 | 126 | 3.4 | | 13 | 6 |
| C3 | 8.4 ± 0.2 | 15 ± 6 | 486 ± 233 | 9.09 ± 1.08 | 285 ± 157 | 5 ± 2 | 136 ± 84 | 122 ± 48 | 0.3 ± 0.1 | 49 ± 22 | 0.03 ± 0.01 | 0.6 ± 0.3 | 26 ± 13 | 18 ± 9 | 2 ± 1 | nd | 13 ± 7 | calcium-magnesium-sulfate-bicarbonate | 0.44 ± 0.14 | 0.02 ± 0.01 | nd | nd | 0.02 | 48 ± 9 | 63 ± 10 | 111 | 3.0 | | 11 | 10 |
| DC-1 | 8.1 ± 0.2 | 42 ± 7 | 2131 ± 74 | 1.13 ± 0.68 | 1174 ± 60 | 168 ± 15 | 361 ± 42 | 409 ± 48 | 2.9 ± 0.1 | 87 ± 16 | 0.15 ± 0.01 | 5.0 ± 0.3 | 294 ± 16 | 34 ± 2 | 27 ± 1 | nd | 11 ± 10 | sodium-sulfate-bicarbonate | 7.12 ± 0.72 | 0.26 ± 0.03 | 4.38 | 0.16 | 0.43 | 570 ± 13 | 279 ± 35 | 849 | 23.0 | x | 9 | 7 |
| DC-2 | 8.4 ± 0.3 | 30 ± 3 | 2077 ± 91 | 3.58 ± 0.63 | 1175 ± 163 | 167 ± 17 | 442 ± 106 | 340 ± 90 | 2.5 ± 0.4 | 71 ± 22 | 0.12 ± 0.02 | 4.5 ± 0.5 | 310 ± 13 | 36 ± 2 | 28 ± 2 | 106 ± - | 29 ± 31 | sodium-sulfate-bicarbonate | 6.26 ± 0.69 | 0.23 ± 0.03 | 3.28 | 0.12 | 0.35 | 436 ± 65 | 183 ± 41 | 619 | 16.7 | x | 14 | 12 |
| DC-3 | 8.4 ± 0.2 | 17 ± 8 | 2980 ± 244 | 8.14 ± 2.69 | 1996 ± 255 | 248 ± 26 | 988 ± 157 | 252 ± 71 | 2.6 ± 0.4 | 82 ± 16 | 0.06 ± 0.02 | 4.5 ± 0.4 | 494 ± 62 | 61 ± 7 | 33 ± 5 | nd | 138 ± 91 | sodium-sulfate | 1.15 ± 0.48 | 0.04 ± 0.02 | nd | nd | 0.04 | 133 ± 58 | 81 ± 14 | 214 | 5.8 | | 10 | 7 |
| DC-4 | 8.5 ± 0.2 | 13 ± 10 | 3239 ± 371 | 8.63 ± 2.14 | 2054 ± 400 | 268 ± 61 | 1001 ± 191 | 340 ± 62 | 2.7 ± 0.5 | 95 ± 12 | 0.05 ± 0.00 | 4.4 ± 0.5 | 540 ± 87 | 67 ± 10 | 33 ± 3 | nd | 7 ± 1 | sodium-sulfate | nd | nd | nd | nd | nd | 73 ± 4 | 78 ± 7 | 151 | 4.1 | | 3 | 4 |
| Reference site | 8.6 ± 0.1 | 7 ± 4 | 2350 ± 1616 | 10.30 ± 1.90 | 1651 ± 1283 | 10 ± 8 | 1021 ± 814 | 319 ± 222 | 0.5 ± 0.1 | 42 ± 26 | 0.11 ± 0.11 | 0.6 ± 0.5 | 510 ± 366 | 10 ± 7 | 5 ± 2 | 499 ± 625 | 11 ± 12 | sodium-sulfate | 0.47 ± 0.07 | 0.02 ± 0.00 | nd | nd | 0.02 | 52 ± 8 | 77 ± 17 | 129 | 3.5 | | 5 | 7 |

*DB-2.0 only 1 sample and thus insufficient number of measurements for SD calculations

**Most sites have insufficient number of measurements for SD calculations

Table S2. Radium loads from NPDES discharges calculated using permit-reported discharge volumes and measured total radium (226+228) and estimating sediment activities using 3 different produced water stream length control volumes.

| Discharge | Avg Discharge Volume (L/s) | Max Discharge Volume (L/s) | Avg Ra 226 (Bq/L) reported | Max Ra 226 (Bq/L) reported | Measured avg Tot Ra (228+226) (Bq/L) | Loads Avg Reported Discharge_Avg reported Ra 226 (g/year) | Tot Ra Loads (Avg Discharge & Measured Tot Ra) (g/year) | Tot Ra Loads (Avg Discharge & Measured Tot Ra) (pCi/year) | Tot Ra Loads (Avg Discharge & Measured Tot Ra) (Bq/year) | Bq/kg sediment/year in $30m^3$ volume (1m wide, 0.30m deep, 100m long) | Bq/kg sediment/year in $4500m^3$ volume (1 m wide, 0.30m deep, 15000m long) | Bq/kg sediment/year in 9000m3 volume (1m wide, 0.30m deep, 30000m long) |
|---|---|---|---|---|---|---|---|---|---|---|---|---|
| DC-1 | 52.1 | 63.5 | 0.35 | 1.06 | 0.43 | 0.016 | 0.019 | 1.89E+10 | 7.0E+08 | 19431 | 130 | 65 |
| DB-2.0 | 3.6 | 47.3 | 0.81 | 1.41 | 2.12 | 0.003 | 0.006 | 6.48E+09 | 2.4E+08 | 6660 | 44 | 22 |
| DA-1 | 141.9 | | 0.24 | | 0.23 | 0.029 | 0.028 | 2.81E+10 | 1.0E+09 | 28919 | 193 | 96 |
| DA-2 | 107.0 | | 0.26 | | 0.19 | 0.024 | 0.018 | 1.76E+10 | 6.5E+08 | 18100 | 121 | 60 |
| DA-3 | 39.9 | | | | 0.39 | 0.000 | 0.013 | 1.31E+10 | 4.9E+08 | 13477 | 90 | 45 |

Table S3. Sediment core porewater concentrations analyzed at each depth interval. Dashed lines indicate non-detectable concentrations.

| Core Site | Depth (cm) | Sr (mg/L ) | Mn (µg/L) | K (mg/L) | Mg (mg/L) | Ca (mg/L) | Fe (µg/L) | Al (mg/L) | Ba (µg/L) | Na (mg/L) | Li (mg/L) | pH | Conductivity (mS/cm) |
|---|---|---|---|---|---|---|---|---|---|---|---|---|---|
| DA-2 | 0 | 7.4 | - | 11 | 83 | 153 | - | - | 45 | 77 | 0.12 | - | |
| | 4 | 8.3 | 103 | 22 | 141 | 478 | - | - | 93 | 229 | 0.24 | 7.8 | 3.42 |
| | 8 | 8.0 | - | 20 | 105 | 363 | - | - | 78 | 188 | 0.20 | 8.0 | 2.73 |
| | 12 | 8.8 | - | 17 | 96 | 353 | - | - | 41 | 149 | 0.18 | 7.8 | 2.53 |
| | 16 | 7.5 | - | 13 | 89 | 334 | - | - | 34 | 131 | 0.17 | 7.8 | 2.38 |
| | 20 | 6.6 | - | 12 | 88 | 341 | - | 0.05 | 34 | 141 | 0.17 | 7.8 | 2.38 |
| | 24 | 5.8 | 79 | 10 | 84 | 353 | - | - | 36 | 146 | 0.17 | 7.7 | 2.49 |
| DC-1 | 0 | 4.3 | - | 32 | 38 | 22 | - | - | 79 | 294 | 0.31 | - | |
| | 6 | 13.6 | - | 48 | 80 | 219 | - | - | 97 | 381 | 0.45 | 8.0 | 3.33 |
| | 10 | 11.2 | - | 40 | 65 | 209 | - | - | 68 | 380 | 0.43 | 8.1 | 3.14 |
| | 14 | 10.5 | - | 44 | 66 | 195 | - | - | 63 | 382 | 0.39 | 8.2 | 3.03 |
| | 18 | 10.3 | 31 | 41 | 70 | 191 | - | - | 73 | 376 | 0.38 | 8.0 | 3.03 |
| | 22 | 11.3 | 120 | 44 | 73 | 219 | - | - | 57 | 395 | 0.39 | 8.2 | 3.12 |
| | 26 | 11.2 | 60 | 43 | 73 | 213 | - | 0.06 | 73 | 403 | 0.42 | 8.3 | 3.12 |
| | 30 | 12.7 | - | 53 | 81 | 243 | - | - | 67 | 444 | 0.47 | 8.4 | 3.32 |
| | 34 | 10.1 | - | 40 | 65 | 196 | - | - | 58 | 408 | 0.42 | 8.4 | 2.92 |
| DB-2.1 | 0 | 6.3 | - | 147 | 105 | 59 | - | - | 36 | 808 | 1.40 | - | |
| | 3 | 16.3 | - | 212 | 165 | 563 | 131 | 0.32 | 113 | 796 | 1.54 | 8.2 | 2.55 |
| | 6 | 15.7 | - | 196 | 166 | 544 | - | - | 138 | 774 | 1.53 | 8.3 | 6.45 |
| | 10 | 13.8 | - | 174 | 154 | 448 | - | 0.06 | 105 | 780 | 1.50 | 8.1 | 6.12 |
| | 14 | 10.8 | - | 154 | 124 | 341 | - | 0.07 | 72 | 754 | 1.41 | 8.1 | 5.52 |
| | 18 | 9.1 | 19 | 147 | 103 | 281 | 314 | 0.19 | 93 | 742 | 1.33 | 8.1 | 5.20 |
| | 22 | 8.6 | - | 167 | 101 | 268 | - | 0.12 | 61 | 782 | 1.33 | 8.4 | 5.29 |
| DC-1 100m | 0 | 4.5 | - | 21 | 38 | 38 | - | 0.32 | 92 | 312 | 0.33 | - | |
| | 6 | 8.3 | 308 | 21 | 65 | 161 | - | - | 47 | 156 | 0.20 | 8.0 | 3.03 |
| | 10 | 6.9 | - | 19 | 60 | 140 | - | - | 25 | 142 | 0.19 | 8.2 | 3.12 |
| | 14 | 16.7 | 28 | 48 | 163 | 373 | 13 | 0.10 | 78 | 395 | 0.53 | 8.3 | 3.12 |
| | 18 | 16.9 | - | 53 | 187 | 407 | - | - | 61 | 452 | 0.62 | 8.4 | 3.32 |
| | 22 | 17.8 | - | 56 | 207 | 445 | - | - | 85 | 485 | 0.68 | 8.4 | 2.92 |
| DA-3 | 0 | 22.0 | - | 20 | 170 | 532 | - | - | 37 | 67 | 0.16 | - | |
| | 4 | 17.4 | - | 53 | 223 | 531 | - | - | 51 | 230 | 0.50 | 7.9 | 4.23 |
| | 8 | 15.4 | - | 51 | 208 | 524 | 24 | - | 63 | 216 | 0.53 | 7.9 | 3.99 |
| | 12 | 14.3 | - | 45 | 202 | 514 | 103 | - | 53 | 222 | 0.55 | 7.9 | 3.97 |
| | 16 | 15.2 | - | 59 | 238 | 595 | 110 | 0.19 | 36 | 254 | 0.68 | 7.8 | 4.47 |

Table S4. Sediment grain size composition as percentages coarse sand, fine sand and silt+clay fractions

| Sample | %coarse sand | %fine sand | %silt+clay |
|---|---|---|---|
| DC-1 | 12 | 65 | 23 |
| DC-2 | 14 | 51 | 33 |
| DC-3 | 31 | 50 | 18 |
| C1 | 92 | 6 | 1 |
| C3 | 16 | 77 | 6 |
| Ref. | 32 | 54 | 13 |
| DB-2.0 | 36 | 46 | 16 |
| DB-2.1 | 61 | 35 | 3 |
| DB-2.2 | 43 | 36 | 19 |

Table S5. Leachate concentrations from DC-1 and DB-2.0 discharges, produced water streams, and local background site samples collected from October 2016. Concentrations were normalized by recovered leachate volumes and original sample mass. Solution blanks per step were left as liquid concentrations. Extraction steps are: (1) soluble salts using ultrapure water; (2) surface exchangeable and low-charge interlayer cations using ammonium acetate buffered to pH 8; (3) carbonate minerals using 8% acetic acid; and (4) high-charge interlayer cations, partial silicates, and oxides using 0.1 M hydrochloric acid.

| Sample | Leach Step | Sr (µg/g) | Mn (µg/g) | K (µg/g) | Mg (µg/g) | Ca (µg/g) | Fe (µg/g) | Al (µg/g) | Ba (µg/g) | Na (µg/g) | pH |
|---|---|---|---|---|---|---|---|---|---|---|---|
| DC-1 | $H_2O$ | 10 | - | 35 | - | 196 | 4 | - | - | 102 | 7.7 |
| | $NH_4OAc$ | 154 | - | 45 | 87 | 3,772 | 3 | - | - | 30 | 8.1 |
| | HOAc | 8,035 | 156 | 12 | 11,531 | 449,083 | 71 | - | 12 | 596 | 5.2 |
| | HCl | 4 | - | 11 | 21 | 540 | 92 | 21 | - | 3 | 2.0 |
| DC-2 | $H_2O$ | 30 | - | 138 | 153 | 767 | 3 | - | - | 395 | 7.5 |
| | $NH_4OAc$ | 145 | 13 | 136 | 339 | 4,308 | 2 | - | 15 | 67 | 8.1 |
| | HOAc | 2,528 | 189 | 22 | 4,694 | 174,610 | 782 | 145 | 120 | 398 | 4.6 |
| | HCl | 44 | 8 | 28 | 165 | 2,021 | 535 | 161 | 5 | 24 | 1.4 |
| DC-3 | $H_2O$ | 23 | 1 | 251 | 181 | 603 | 3 | - | - | 501 | 7.6 |
| | $NH_4OAc$ | 144 | 38 | 371 | 654 | 4,370 | 2 | - | 39 | 93 | 8.1 |
| | HOAc | 40 | 177 | 39 | 3,178 | 11,595 | 376 | 64 | - | 45 | 3.6 |
| | HCl | 8 | 31 | 100 | 810 | 2,398 | 873 | 390 | 8 | 33 | 1.3 |
| C1 | $H_2O$ | - | - | 27 | - | 143 | 4 | 7 | - | 26 | 7.8 |
| | $NH_4OAc$ | 3 | 7 | 34 | 54 | 1,663 | 2 | 3 | 7 | 22 | 8.1 |
| | HOAc | - | 46 | 24 | 408 | 2,783 | 109 | 59 | 1 | 58 | 3.1 |
| | HCl | - | 11 | 29 | 58 | 561 | 269 | 177 | 2 | 42 | 1.2 |
| C3 | $H_2O$ | - | - | 32 | 15 | 188 | 4 | 3 | - | 62 | 7.4 |
| | $NH_4OAc$ | 13 | 10 | 58 | 214 | 2,734 | 2 | 2 | 15 | 23 | 8.1 |
| | HOAc | - | 65 | 38 | 1,710 | 6,311 | 273 | 70 | 2 | 47 | 3.3 |
| | HCl | 0 | 12 | 34 | 366 | 1,819 | 441 | 327 | 5 | 46 | 1.3 |
| Reference | $H_2O$ | - | - | 66 | - | 87 | 25 | 40 | - | 288 | 7.8 |
| | $NH_4OAc$ | 48 | 4 | 295 | 277 | 4,435 | 2 | - | 44 | 120 | 8.1 |
| | HOAc | 9 | 140 | 26 | 2,678 | 11,094 | 82 | 89 | - | 60 | 3.6 |
| | HCl | 2 | 31 | 58 | 583 | 2,184 | 284 | 310 | 1 | 42 | 1.3 |
| DB-2.0 | $H_2O$ | 79 | - | 209 | 155 | 3,805 | 8 | - | - | 342 | 6.9 |
| | $NH_4OAc$ | 81 | - | 66 | 61 | 4,927 | 6 | - | 24 | 68 | 8.1 |
| | HOAc | 2,406 | 31 | 200 | 1,787 | 261,639 | 429 | 10 | - | 644 | 4.8 |
| | HCl | 22 | 2 | 44 | 792 | 2,476 | 562 | 374 | 7 | 14 | 1.8 |
| DB-2.1 | $H_2O$ | 3 | - | 226 | 22 | 306 | 4 | 2 | - | 465 | 7.3 |
| | $NH_4OAc$ | 57 | 3 | 111 | 154 | 4,160 | 2 | 3 | 6 | 57 | 8.1 |
| | HOAc | 140 | 116 | 33 | 1,532 | 53,300 | 471 | 38 | 4 | 71 | 4.0 |
| | HCl | 0 | 6 | 55 | 5,281 | 9,468 | 163 | 80 | 1 | 35 | 1.8 |
| DB-2.2 | $H_2O$ | - | - | 95 | - | 83 | 3 | - | - | 495 | 8.1 |
| | $NH_4OAc$ | 75 | 9 | 253 | 495 | 4,634 | 2 | - | 23 | 130 | 8.1 |
| | HOAc | 5 | 159 | 3 | 3,422 | 31,042 | 46 | 49 | - | 28 | 3.8 |
| | HCl | - | 12 | 49 | 756 | 2,848 | 160 | 198 | - | 25 | 1.4 |
| | | Sr (mg/L) | Mn (mg/L) | K (mg/L) | Mg (mg/L) | Ca (mg/L) | Fe (µg/L) | Al (mg/L) | Ba (mg/L) | Na (mg/L) | pH |
| Solution Blanks | $H_2O$ | - | - | - | - | - | 131 | - | - | - | 7.0 |
| | $NH_4OAc$ | - | - | - | - | - | 145 | - | - | - | 8.0 |
| | HOAc | - | - | - | - | - | 539 | - | - | - | 2.7 |
| | HCl | - | - | - | - | - | 102 | - | - | - | 1.2 |

Table S6. Corresponding values of fraction of water remaining, concentration factor, and moles of water removed for progressive evaporation model using PHREEQC.

| Moles water per kilogram solution | Moles water evaporated per kilogram solution | Water fraction evaporated | Water fraction remaining | Concentration factor for conservative solute | Incremental moles of water removed |
|---|---|---|---|---|---|
| 55.506 | 0.000 | 0 | 1 | 1.000 | 0.0000 |
| 49.955 | 5.551 | 0.1 | 0.9 | 1.111 | 5.5506 |
| 44.405 | 11.101 | 0.2 | 0.8 | 1.250 | 5.5506 |
| 38.854 | 16.652 | 0.3 | 0.7 | 1.429 | 5.5506 |
| 33.304 | 22.202 | 0.4 | 0.6 | 1.667 | 5.5506 |
| 27.753 | 27.753 | 0.5 | 0.5 | 2.000 | 5.5506 |
| 22.202 | 33.304 | 0.6 | 0.4 | 2.500 | 5.5506 |
| 16.652 | 38.854 | 0.7 | 0.3 | 3.333 | 5.5506 |
| 11.101 | 44.405 | 0.8 | 0.2 | 5.000 | 5.5506 |
| 5.551 | 49.955 | 0.9 | 0.1 | 10.000 | 5.5506 |
| 2.775 | 52.731 | 0.95 | 0.05 | 20.000 | 2.7753 |
| 2.220 | 53.286 | 0.96 | 0.04 | 25.000 | 0.5551 |
| 1.665 | 53.841 | 0.97 | 0.03 | 33.333 | 0.5551 |
| 1.110 | 54.396 | 0.98 | 0.02 | 50.000 | 0.5551 |
| 0.555 | 54.951 | 0.99 | 0.01 | 100.000 | 0.5551 |
| 0.056 | 55.450 | 0.999 | 0.001 | 1000.000 | 0.4996 |